Article

Neuron

Cortical Feedback Decorrelates Olfactory Bulb Output in Awake Mice

Highlights

- Piriform feedback to olfactory bulb is sparse, odor specific, and locally diverse
- Distinct feedback axon types enhance or suppress their baseline activity to odors
- Feedback responses are layer selective and can outlast odor stimulation by seconds
- Piriform cortex decorrelates mitral but not tufted cells' odor responses

Authors

Gonzalo H. Otazu, Honggoo Chae, Martin B. Davis, Dinu F. Albeanu

Correspondence

albeanu@cshl.edu

In Brief

Otazu, Chae et al. describe sparse and odor-specific piriform cortex feedback to olfactory bulb. They find that distinct feedback axonal types are either enhanced or suppressed by odors. Cortical inactivation differentially decorrelates mitral, but not tufted cells odor representations.

Otazu et al., 2015, Neuron *86*, 1461–1477
June 17, 2015
http://dx.doi.org/10.1016/j.neuron.2015.05.023

CellPress

Neuron
Article

Cortical Feedback Decorrelates Olfactory Bulb Output in Awake Mice

Gonzalo H. Otazu,[1,3] Honggoo Chae,[1,3] Martin B. Davis,[1] and Dinu F. Albeanu[1,2,*]
[1]Cold Spring Harbor Laboratory, Cold Spring Harbor, NY 11724, USA
[2]Watson School of Biological Sciences, Cold Spring Harbor, NY 11724, USA
[3]Co-first author
*Correspondence: albeanu@cshl.edu
http://dx.doi.org/10.1016/j.neuron.2015.05.023

SUMMARY

The olfactory bulb receives rich glutamatergic projections from the piriform cortex. However, the dynamics and importance of these feedback signals remain unknown. Here, we use multiphoton calcium imaging to monitor cortical feedback in the olfactory bulb of awake mice and further probe its impact on the bulb output. Responses of feedback boutons were sparse, odor specific, and often outlasted stimuli by several seconds. Odor presentation either enhanced or suppressed the activity of boutons. However, any given bouton responded with stereotypic polarity across multiple odors, preferring either enhancement or suppression. Feedback representations were locally diverse and differed in dynamics across bulb layers. Inactivation of piriform cortex increased odor responsiveness and pairwise similarity of mitral cells but had little impact on tufted cells. We propose that cortical feedback differentially impacts these two output channels of the bulb by specifically decorrelating mitral cell responses to enable odor separation.

INTRODUCTION

Early sensory areas receive massive top-down projections from the cortex, suggesting that this feedback plays a crucial function (Otazu and Leibold, 2011; Rao and Ballard, 1999). Visual, auditory, and somatosensory experiments have proposed several roles for cortical feedback, including sharpening of sensory representations, or relaying information pertaining to expectation, reward, attention, learning, and action (Gilbert and Li, 2013; Glickfeld et al., 2013; Harris and Mrsic-Flogel, 2013; Petreanu et al., 2012). The olfactory bulb (OB), like other early sensory areas, receives abundant feedback projections from cortical areas involved in odor identification, localization, and olfactory memory (Boyd et al., 2012; Markopoulos et al., 2012; Oswald and Urban, 2012; Shepherd, 1972). Although cortical feedback axons outnumber olfactory sensory inputs, their function in shaping the OB output remains unclear to date.

The OB receives glutamatergic feedback mainly from anterior olfactory nucleus (AON), piriform, and entorhinal cortex (Oswald and Urban, 2012; Rothermel and Wachowiak, 2014; Shepherd, 1972; Shipley and Adamek, 1984). The bulb also integrates GABAergic (Nunez-Parra et al., 2013), neuromodulatory (Devore and Linster, 2012; Petzold et al., 2009; Ranade and Mainen, 2009; Wachowiak et al., 2009; Wilson et al., 2004), and hormonal (Tobin et al., 2010) inputs that have been proposed to contextually regulate OB activity during learning and odor discrimination. In this study, we focus on understanding the dynamics and roles of feedback signals from the primary olfactory cortex (piriform) to the bulb.

Previous work has suggested that in complex sensory environments, the piriform cortex reconstructs olfactory objects from degraded noisy stimuli or segments relevant targets from irrelevant, variable backgrounds (Gottfried, 2010; Vickers, 2000; Wilson and Sullivan, 2011). Within this framework, the piriform cortex may act as a pattern-recognition device (Babadi and Sompolinsky, 2014; Barak et al., 2013; Caron et al., 2013; Haberly, 2001; Haberly and Bower, 1989; Linster and Hasselmo, 2001) that compares incoming sensory inputs with representations of previously experienced odors, integrates contextual information, and sends predictive signals to the sensory periphery through massive bulbar feedback projections. Indeed, anatomical tracing studies show that individual anterior piriform cortex (APC) feedback axons follow long, tortuous trajectories across the OB and form clusters of synapses that can lie far apart from each other (Matsutani, 2010).

The output neurons of the OB, the mitral/tufted (MT) cells, project most abundantly in a distributed manner to the piriform cortex and to several other areas including the AON, olfactory tubercle, entorhinal cortex, and amygdala (Ghosh et al., 2011; Miyamichi et al., 2011; Nagayama et al., 2010; Shepherd, 1972; Sosulski et al., 2011). In turn, the primary recipients of these feedback projections are the granule cells (GCs) (Balu et al., 2007; Boyd et al., 2012; Margrie et al., 2001; Urban and Sakmann, 2002; Wilson and Mainen, 2006). Piriform cortex feedback axons also establish sparser synapses with deep short axon cells, which inhibit the GCs, and with interneurons in the glomerular layer (periglomerular and superficial short axon cells) (Boyd et al., 2012; Matsutani, 2010). Thus, cortical feedback axons act indirectly on MT cells via OB inhibitory interneurons.

Studies in anesthetized rodents have proposed that cortical feedback provides non-specific, global inhibitory gain control to prevent runaway saturation of MT cell firing. Electrical

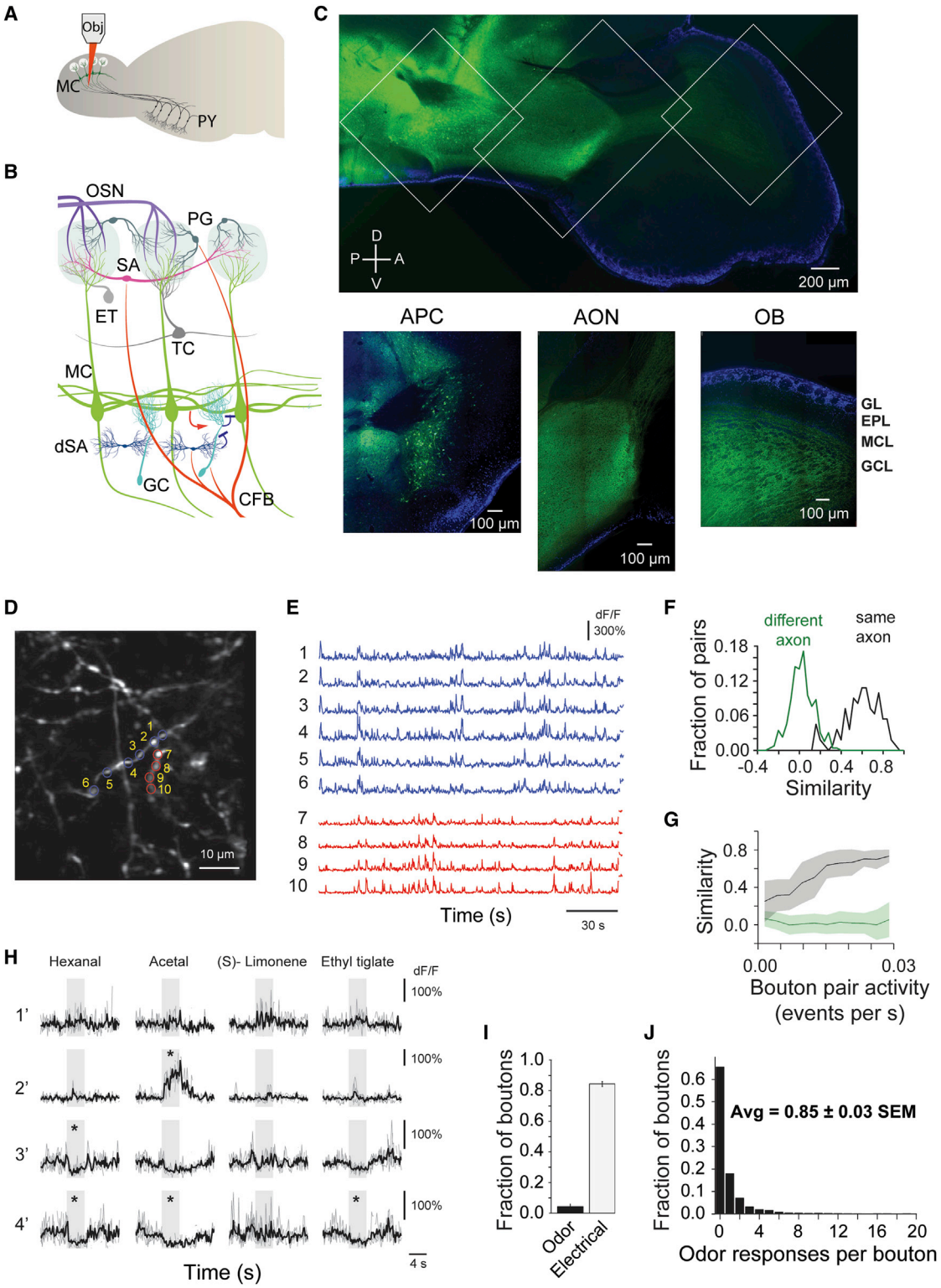

Figure 1. Monitoring Corticalbulbar Boutons in Awake Head-Fixed Mice via Multiphoton Imaging of GCaMP5 Signals

(A) Schematics of experimental setup: optical monitoring of cortical-bulbar feedback bouton responses via multiphoton imaging of GCaMP5 signals; Obj, 2p microscope objective; MC, mitral cells; Py, pyramidal neurons in the anterior piriform cortex (APC).

(B) Olfactory bulb (OB) circuit and neuronal types; OSN, olfactory sensory neurons; PG, periglomerular cells; SA, superficial short axon cells; ET, external tufted cells; TC, tufted cells; MC, mitral cells; dSA, deep short axon cells; GC, granule cells; CFB, cortical feedback fibers.

(legend continued on next page)

(Nakashima et al., 1978) or optogenetic (Boyd et al., 2012) activation of the feedback projections has been shown to suppress odor-evoked MT cell responses. These results cannot easily be extrapolated to awake animals, since cortical feedback could be modulated by context and expectation and may follow substantially different dynamics (Gilbert and Li, 2013; Harris and Mrsic-Flogel, 2013). In addition, piriform cortex inactivation in awake rabbits has been shown to synchronize MT cells, while decreasing their firing rate, which contradicts the findings from anesthetized mice (Gray and Skinner, 1988).

To date, it remains unknown whether the impact of piriform cortex feedback varies across the two main output populations of the bulb, the mitral and tufted cells, which reside in different anatomical layers. Recent work indicates that mitral and tufted cells differ in response properties (Burton and Urban, 2014; Fukunaga et al., 2012; Igarashi et al., 2012; Manabe and Mori, 2013; Nagayama et al., 2004) and project differentially to downstream brain areas, with stronger tufted cell innervation of the AON compared to the piriform cortex (Igarashi et al., 2012).

Here, we characterized the response properties of cortical bulbar boutons in awake head-fixed mice across bulb layers as a function of odor identity and concentration via multiphoton imaging of GCaMP5 signals (Figures 1A and 1B). Furthermore, we employed pharmacological suppression of neuronal activity in the APC in conjunction with optical monitoring of both mitral and tufted cells activity to determine the contribution of top-down cortical inputs in shaping sensory processing in the bulb.

RESULTS

We expressed the genetically encoded calcium indicator GCaMP5 (Tian et al., 2009) in the APC under the control of the *EF1α* promoter using adeno-associated viruses (AAV2.9). To ensure homogeneous labeling of the APC, we performed multiple bilateral injections (see Experimental Procedures). Confocal imaging of DAPI signals and GCAMP5 fluorescence in sagittal slices showed robust labeling of cell bodies in the APC and abundant neuropil in the OB and AON (Figure 1C; Figure S1A). No fluorescent cell bodies could be detected in the OB. In the bulb, the density of GCaMP5-labeled boutons was highest in the GCL, but axonal projections were also present in the glomerular and external plexiform layers (Figures 1B and 1C; Figures S1C and S1D). Consistent with previous reports of lack of GABAergic feedback from the piriform cortex (Boyd et al., 2012), we did not find expression of GCaMP5 in feedback axons upon injection of *EF1α-FLEX-GCaMP5* AAV2.9 in the APC of *GAD65*-Cre mice (Figure S1B; Taniguchi et al., 2011).

Corticalbulbar Feedback Projections Are Spontaneously Active and Show Sparse and Odor-Specific Responses

To date, little is known about corticobulbar feedback activity in awake or anesthetized animals. One recent study investigated the dynamics of AON-to-bulb feedback boutons in the glomerular layer (Rothermel and Wachowiak, 2014). As a first step toward understanding the functional roles of corticalbulbar feedback projections, we characterized their spontaneous dynamics and responses to a diverse panel of 20 odors (Odor Set A, Table S1), using multiphoton imaging of GCaMP5 signals in awake head-fixed mice (Figures 1A and 1D; Figures S1E–S1G, see Experimental Procedures). We started by monitoring feedback axons innervating the deep OB layers (200–350 μm from surface), since these represent the highest number of corticalbulbar projections (Figures S1C and S1D).

Approximately 23% of the imaged boutons (5,221 boutons, 18 fields of view, 4 mice) showed locally diverse and brief (<1 s) spontaneous activity bouts (Figures 1D and 1E, Figures S1H, S2A, and S2B, Movie S1, see Experimental Procedures). Boutons anatomically assigned to the same axonal branch (see Experimental Procedures) showed significantly higher correlations than boutons belonging to different branches in a given field of view (FOV) (average = 0.60 ± 0.02 versus average = 0.03 ± 0.01, values indicate mean ± SEM unless specified otherwise, 52 axonal segments, 337 pairs of boutons from the same axon, 648 pairs of boutons from different axons, $p < 0.001$, Wilcoxon rank-sum test, Figures 1F and 1G; Figure S1H). As expected, correlations in spontaneous activity of boutons on the same axon (Petreanu et al., 2012) were higher for bouton pairs that had high levels of spontaneous activity (Figure 1G).

To determine whether an odor response was significant, we compared the average fluorescence change during odor presentation with a bootstrap distribution of average fluorescence calculated over baseline periods of equal length preceding odor presentation (threshold = 99.9th percentile of bootstrap

(C) Top: composite GCaMP5 (green) and DAPI nuclear (blue) signals in a confocal reconstruction tiling a fixed sagittal brain slice from a mouse injected in the APC with AAV2.9 *GCaMP5*-expressing viruses. Bottom: insets for APC (left), anterior olfactory nucleus (AON) (center), and OB (right); GL, glomerular laye;, EPL, external plexiform layer; MCL, mitral cell layer; GCL, granule cell layer; A, anterior; P, posterior; D, dorsal; V, ventral.

(D) Example field of view ~300 μm deep from surface of GCaMP5 labeled cortical feedback axons and boutons in an awake head-fixed mouse.

(E) Spontaneous activity traces (dF/F_0) from feedback boutons marked in (D). Top six traces and respectively bottom four traces are from boutons of two different axonal branches.

(F) Histogram of pairwise correlations of baseline activity (dF/F) in a 3 min interval preceding odor presentation; green and black traces corresponds to bouton pairs from different and respectively same axonal branches.

(G) Pairwise correlations of baseline activity (dF/F) in a 3 min interval preceding odor presentation as a function of spontaneous events frequency; shaded area corresponds to standard deviation.

(H) Odor responses of four example boutons in GCL across four different stimuli (hexanal, acetal, [S]-limonene, ethyl tiglate, 0.4% saturated vapor pressure). Individual repeats (gray) and average traces (black) are shown; odors trigger both positive (enhanced responses) and negative (suppressed responses) deflections from baseline; * marks significant odor responses; stimulus duration, 4 s.

(I) Average fraction of cortical feedback boutons imaged responsive to odor (Odor) and APC electrical stimulation (Electrical) (40 pulses, 100 μs, at 100 Hz, 30 μA); error bars indicate SEM calculated over odors and fields of view (left) and fields of view respectively (right).

(J) Histogram of the number of odors in the panel (Odor Set A, Table S1) that individual feedback boutons in the GCL responded to.

fluorescence distribution; Figures S2C–S2F; see Experimental Procedures). Odor presentation triggered significant responses in ~35% of all imaged boutons (responsive to at least one odor, Figure 1H). A given odor in the panel (Odor Set A, Table S1), on average, triggered responses in only 4.3% ± 0.4% (N = 20 odors) of cortical feedback boutons imaged in the GCL (5,221 boutons, 18 FOVs, 4 mice), and on average a bouton responded to 0.85 ± 0.03 odors (Figures 1I and 1J). Within the subset of responsive boutons, individual boutons responded sparsely (2.5 ± 0.07, odor responses/bouton, N = 1,827 responsive boutons) through enhancement (~45%) and more often suppression (~55%) of baseline activity (4,412 odor-bouton pairs, 4 mice, Movies S2 and S3). The distribution of number of odor responses per bouton did not follow a single binomial distribution, suggesting the presence of distinct populations of highly selective, as well as more promiscuous feedback boutons (Figures S2G and S2H).

A direct comparison of activity patterns from the same boutons across anesthetized and awake conditions showed significant reduction in spontaneous events during anesthesia (ketamine/xylazine, see Experimental Procedures, 4.6 ± 0.4 spontaneous events per 3 min interval versus 10.2 ± 0.5, N = 283 boutons, 2 mice, $p < 0.001$, Wilcoxon signed-rank test; Figures S3A and S3B). Suppressed odor responses were weaker under anesthesia (Stettler and Axel, 2009) (~84% of suppressed responses were weaker, N = 112, $p < 0.001$, Wilcoxon signed-rank test; Figure S3C). Enhanced responses showed both increases and decreases in response amplitude and number of responsive boutons under anesthesia (N = 326 bouton-odor pairs, 2 mice; Figures S3C and S3D), and on average were stronger (Figure S3C) and more robust across trials (SD / mean response = 1.2 ± 0.09 awake versus 0.72 ± 0.09 anesthetized, $p < 0.001$, Wilcoxon signed-rank test). In anesthetized mice, a given odor triggered responses in an average of 7.42% ± 0.22% of imaged feedback boutons in the GCL (N = 326 responsive bouton-odor pairs, 2 mice), similar in range to reports monitoring responses in cell bodies from the piriform cortex (Stettler and Axel, 2009). Corticalbulbar feedback activity depends heavily on the brain state. Thus, for the rest of this study, we restricted experiments to awake, head-fixed mice.

To determine whether the sparse nature of observed feedback odor responses can be accounted for by poor cell health (from viral GCaMP5 expression) or limited sensor sensitivity, we electrically stimulated the APC (8 × 100 μs pulses, 100 Hz, 30 μA, see Experimental Procedures) while monitoring feedback responses. Electrical stimulation evoked strong and long-lasting calcium transients in the majority of boutons (85%; Figure 1I; Figures S4A and S4C), likely due to dense recurrent connections in the APC (Franks et al., 2011).

To assess the relationship between neuronal spike rate and fluorescence measurements, we similarly monitored the change in GCaMP5 signals in corticalbulbar feedback boutons in response to electrical stimulation in the APC (100 μs, 50 μA, see Experimental Procedures) of awake mice. To eliminate the contribution of intra-cortical recurrent activity to the GCaMP5 responses, we performed these experiments in conjunction with local injection of the $GABA_A$ receptor agonist muscimol in the APC (0.5 mg/ml, 1 μl over 5 min, see Experimental Procedures). Using fluorescent muscimol (1.0 mg/ml, 2 μl over 10 min, see Experimental Procedures), in a subset of experiments (N = 3 mice), we confirmed that muscimol spread was restricted to the APC and did not diffuse to nearby cortical areas such as the AON (see Experimental Procedures; Figures S5B and S5C). Muscimol injection significantly decreased the frequency of spontaneous events (Figures S5D and S5E) in cortical feedback boutons and completely abolished odor-evoked bouton responses (Figure S5F).

In the presence of muscimol, single pulses (100 μs, 50 μA, see Experimental Procedures) failed to evoke calcium transients, suggesting that GCaMP5 activity may not report single action potentials (Akerboom et al., 2012). However, pairs of pulses, as well as stronger stimulation protocols did evoke detectable fluorescence transients (Figures S5G and S5H) with response kinetics matching reports from cultured neurons (~120 ms onset, ~250 ms offset, Figures S5G, S5J, and S5K). The amplitude of evoked calcium transients (dF/F) increased monotonically with the number of pulses per stimulation event (2–16 pulses at 50 Hz or 100 Hz) and spanned the range of dF/F values observed for bouton odor responses (Figure S5H).

Pyramidal neurons in the piriform cortex have been reported to fire spontaneous bursts of 2–5 spikes at high frequency (≥100 Hz) (McCollum et al., 1991). Spontaneous calcium transients in our data (Figures 1E and S1H) match the increase in fluorescence amplitude triggered by electrical stimulation bursts (2–16 pulses at 50 or 100 Hz, Figure S5H). These observations suggest that calcium transients observed in the corticalbulbar boutons, at rest, represent short bursts of several action potentials and may indeed reflect the ongoing spontaneous activity of pyramidal APC neurons.

To estimate the relationship between decreases in fluorescence during odor-evoked suppression and changes in neuronal firing rate, we obtained an estimate of the expected baseline bouton fluorescence given various rates of spontaneous activity. To this end, we convolved the average dF/F bouton response to APC electrical stimulation in the presence of muscimol (2 pulses, 100 μs, 50 μA, 100 Hz) with Poisson pulse trains of different frequencies (Figure S5I). We found that the amplitude of odor-suppressed responses was consistent with the fluorescence change calculated from a simulated average spike rate of a few Hz (Figure S5I), suggesting that the suppression in bouton fluorescence may reflect the silencing of spontaneous firing bouts in the APC (Zhan and Luo, 2010).

Two Distinct Corticalbulbar Feedback Channels: Enhanced versus Suppressed Boutons

Strikingly, boutons showed high selectivity in their mode of response (enhancement versus suppression). Approximately 40% of the responsive boutons reacted to odors exclusively by enhancement and 55% by suppression of their baseline activity (Figures 2A–2D). This dichotomy in response was present throughout the population, and became even more apparent when the analysis was restricted to boutons that were responsive to more than half of odors in the panel (0 out of 52 boutons showed mixed responses). The sparse nature and segregation of enhanced and suppressed responses remained apparent even when sampling a larger odor panel (33 odors, Odor Set B,

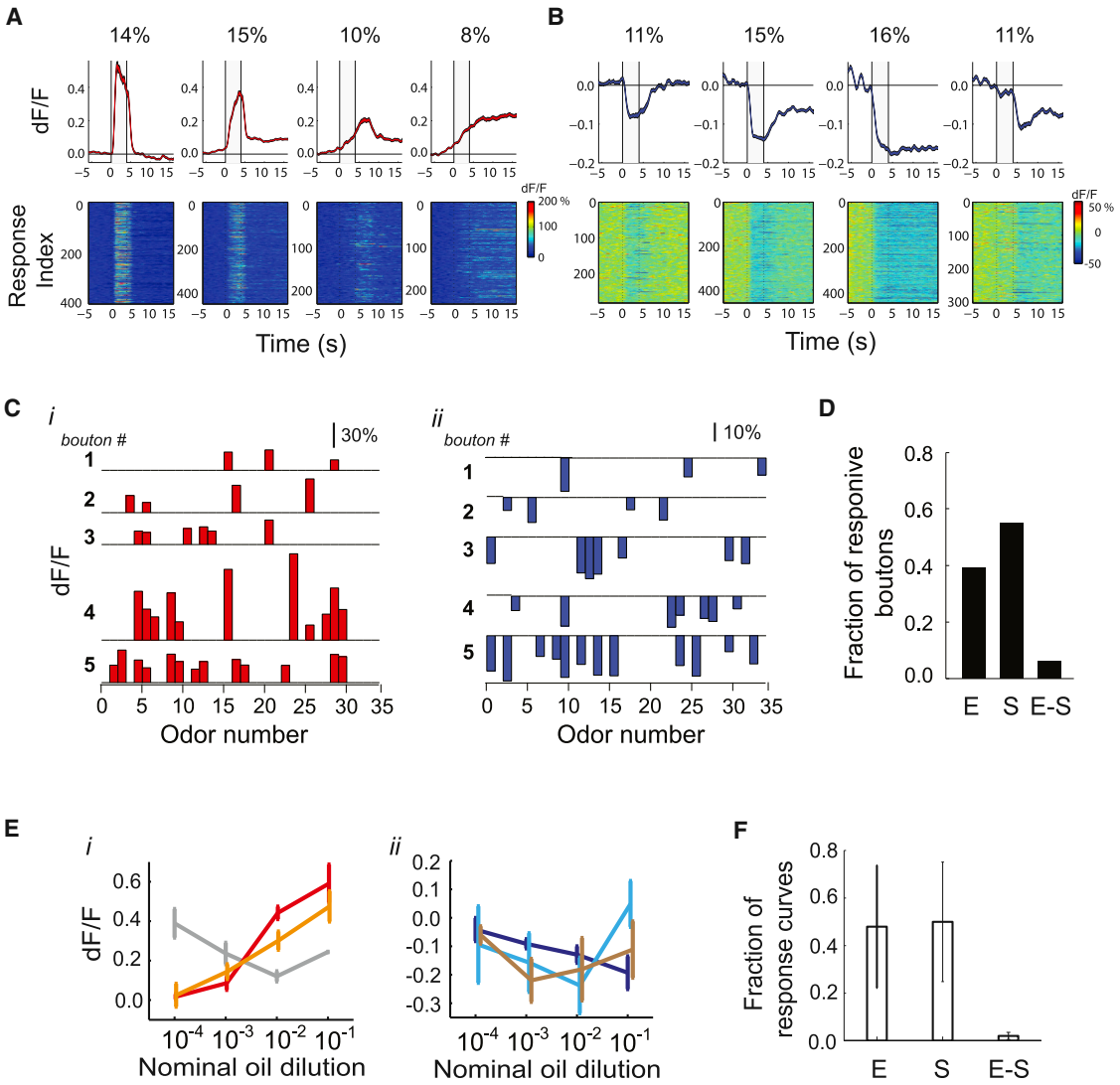

Figure 2. Dichotomy in Corticalbulbar Feedback Odor Responses: Enhanced versus Suppressed Boutons

(A and B) Odor response types obtained via k-means clustering and their relative distribution in the population of feedback boutons targeting the GCL; average response shapes (top) and all corresponding odor responses (GCaMP5) assigned to each cluster (bottom). (A) Enhanced response clusters; (B) suppressed response clusters.

(C) Example average odor response spectra (ORS) of enhanced (red) and suppressed (blue) boutons; sparsely responding boutons, as well as broadly tuned boutons are shown for illustration.

(D) Fraction of boutons responsive to odors in the panel (Odor Set A, Table S1) via only enhancement (E), only suppression (S), and both enhancement and suppression (E-S);

(E) Enhanced (i) and suppressed (ii) concentration-response (GCaMP5) curves for two odors (ethyl valerate, i, and heptanal, ii) in three example cortical feedback boutons; error bars indicate SEM across repeats.

(F) Fraction of concentration response curves that were purely enhanced (E), only suppressed (S), or showed both enhancement and suppression compared to baseline within the sampled concentration range (E-S); error bars indicate SD across fields of view.

Table S1; ~6.7% of responsive boutons showed both enhanced and suppressed responses, N = 856 boutons, 2 mice; Figure 2C, Figure S4D) and could not be easily explained by odor sampling biases. On average, suppressed boutons were as narrowly tuned to odors as enhanced boutons (average lifetime sparseness suppressed boutons = 0.60 ± 0.30 SD, N = 849 boutons versus 0.60 ± 0.23 SD, N = 849 enhanced boutons, p = 0.95, Wilcoxon rank-sum test). Furthermore, boutons belonging to the same axon consistently showed either enhanced or suppressed odor responses (only 1 out of 52 analyzed axons had mixed responses), suggesting that the polarity of response segregates along different axons.

Suppressed boutons were more active in the baseline period (0.017 ± 0.001 events/s versus 0.010 ± 0.001 events/s, $p < 0.001$, t test) and displayed higher resting fluorescence (F_0) compared to enhanced boutons (Figures S4E–S4G). The lack

of excitatory odor responses in these boutons may simply result from baseline saturation of the GCaMP5 sensor. Conversely, the absence of negative deflections in the "enhanced" boutons could be explained by an intrinsic bias in calcium imaging methods toward detecting increases in fluorescence, given low resting activity. However, several pieces of evidence render these possibilities unlikely (Supplementary Note 1, Experimental Procedures, Figures S4E–S4H). In addition, we directly tested whether boutons suppressed by odors can in principle show an increase in their baseline fluorescence levels via APC electrical stimulation (see Experimental Procedures). Brief electrical stimulation (100 μs at 30 μA) during periods of odor-triggered suppression reliably resulted in increased fluorescence, switching the response polarity of individual boutons from suppression to enhancement (Figures S4A–S4C). This robust fluorescence increase upon electrical stimulation (Figure 1I) confirms that the observed dichotomy of suppressed and enhanced bouton odor responses is not an artifact of sensor saturation and may instead represent different selective populations of pyramidal cells in the APC that respond to odors mostly via enhancement or via suppression.

Corticalbulbar Feedback Responses Often Outlast Stimulus Presentation

Clustering of odor responses (see Experimental Procedures) revealed diverse temporal dynamics of both enhanced and suppressed bouton responses, including "transient," "ramping," "persistent," and "lingering" features (Figures 2A and 2B, 18 FOV, 4 mice, 2,913 odor-bouton pairs). On average, enhanced responses tracked stimulus dynamics and changes in concentration more closely. Many boutons showed long-lasting activity patterns that outlasted the odor stimulus (4 s) by several seconds (>12 s) (76% of suppressed boutons, 35% of enhanced boutons). Further, ~20% of both suppressed and enhanced responses were triggered by the termination of odor stimulation (OFF responses). Given the GCaMP5 faster response kinetics (Figures S5G, S5J, and S5K), these observations indicate that brief odor inputs can initiate long-lasting bouts of activity in cortical feedback fibers which may further impact bulbar dynamics during fluctuating odor plumes or across multiple encounters of the same stimulus.

Separation of Enhanced and Suppressed Bouton Responses Is Maintained across Odor Concentrations

We investigated whether the dichotomy of bouton response types is particular to the odor concentrations used, or present across a wider range of stimulus intensities. Computational (Kaplan and Lansner, 2014; Wilson and Sullivan, 2011) and experimental (Franks et al., 2011; Stettler and Axel, 2009) studies in anesthetized mice have suggested that the piriform cortex shows invariance to changes in odor concentration. We sampled odor concentration (Figure 2E; Figures S6A and S6B; see Experimental Procedures) across ~3 orders of magnitude (Figure S6A). Only 10% of bouton responses were concentration invariant (changed average response amplitude across concentrations within the range of inter-trial variability, see Experimental Procedures; Figure S6C; 309/4,940 boutons, 6,582 bouton-concentration responses, 12 FOVs, 3 mice). Varying stimulus strength modulated both the amplitude and number of bouton responses (Figure 2E; Figure S6). Across concentrations, some boutons showed monotonic increase/decrease in response amplitude, while others (~50%) followed complex non-monotonic response curves (see Experimental Procedures; Figures S6D–S6F). Importantly, within the sampled concentration range, we rarely (<5%) observed a change in the response of the feedback boutons targeting the GCL from enhanced to suppressed and vice-versa (Figure 2F).

Differential Cortical Feedback Dynamics across Bulb Layers

In addition to targeting the GCL, corticalbulbar feedback fibers synapse sparsely on inhibitory interneurons in the glomerular layer (GL) as well (Figures 1C and 3A; Figures S1C and S1D). We tested whether the activity patterns and spatial organization of cortical feedback vary across bulb layers. Feedback boutons in the GL appeared to have more spontaneous activity compared to the ones in GCL (average = 14.9 ± 0.2 events per 3 min, N = 3,355 boutons, 10 FOVs, 6 mice versus 1.62 ± 0.1, N = 5,067, 14 FOVs, 4 mice; Figure 3B; Figure S7A). A possible explanation for this discrepancy is the increased optical access to the superficial glomerular layer compared to the deeper granule cell layer. This apparent increase in baseline fluorescence can in principle facilitate the detection of suppressed odor responses. However, the GL feedback boutons were sparser in their responses (Figures 3C and 3D) compared to the deeper layers (average lifetime sparseness = 0.72 ± 0.23 SD, N = 558 responsive boutons in GL versus 0.61 ± 0.27 SD, N = 1,527 boutons in GCL, within same animals, $p < 0.001$, Wilcoxon rank-sum test). Specifically, purely suppressed boutons were significantly narrower in their tuning compared to their counterparts in the GCL (average lifetime sparseness = 0.81 ± 0.21 SD, N = 296 boutons in GL versus 0.60 ± 0.21 SD, N = 849 boutons in GCL, $p < 0.001$, Wilcoxon rank-sum test), while the enhanced boutons were matched in broadness of tuning across layers (average lifetime sparseness = 0.61 ± 0.21 SD, N = 228 GL boutons versus 0.60 ± 0.23 SD, N = 632 GCL boutons, $p = 0.86$, Wilcoxon rank-sum test; Figures 3C and 3D). Mixed boutons were a minority in the GL as well, but appeared more frequently compared to the GCL (14% E-S; Figure S7B). Clustering revealed several types of odor responses across the population, similar to those observed in the GCL with a significant fraction of responses outlasting stimulus offset (~48% of suppressed, ~34% of enhanced responses, Figures S7C and S7D). Thus, across bulb layers, cortical bulbar feedback fibers differ in the frequency of suppressed responses but are similar in the presence of enhanced-suppressed bouton dichotomy and long-lasting responses.

Local Diversity in Cortical Feedback Representations across Odors

To determine whether cortical feedback is locally tuned or spatially distributed, we computed the degree of overlap in the odor responses of pairs of nearby and distant boutons monitored simultaneously. We first investigated the relationship between similarity of odor response spectra (correlation coefficient) and physical separation in the GCL boutons (Soucy et al., 2009).

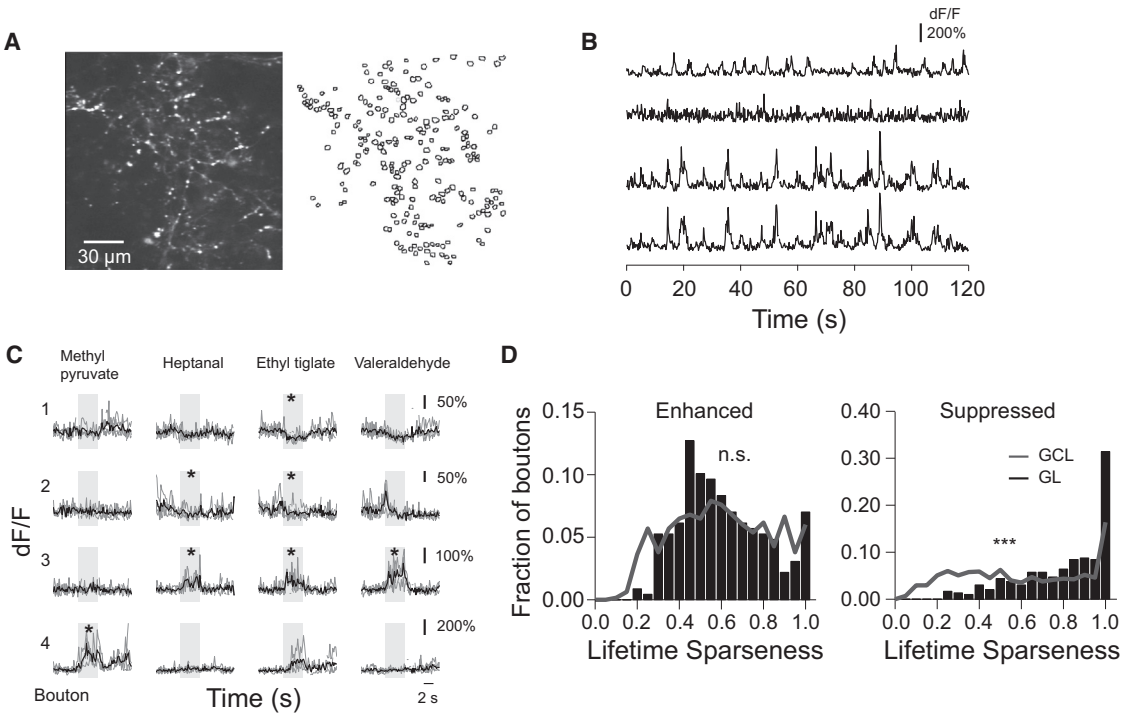

Figure 3. Differential Cortical Feedback Bouton Odor Responses across Bulb Layers

(A) Left: example field of view ~80 μm deep from surface of GCaMP5 labeled cortical feedback axons and boutons in an awake head-fixed mouse; right: outlines of the regions of interest (ROIs) corresponding to putative cortical feedback boutons.

(B) Spontaneous activity traces from the feedback boutons selected in the field of view showed in (A). Bottom two traces correspond to boutons assigned to the same axonal branch by reconstruction of single axons.

(C) Odor responses of four example boutons in GL across four different stimuli (ethyl pyruvate, heptanal, ethyl tiglate, valeraldehyde, 0.4% saturated vapor pressure). Individual repeats (gray) and average traces (black) are shown; odors trigger both positive (enhanced responses) and negative (suppressed responses) deflections from baseline; * mark significant odor responses; stimulus duration, 4 s.

(D) Lifetime sparseness of boutons responsive to odors in the panel (Odor Set A, Table S1) only via enhancement (left) or suppression (right); distributions in the GCL (black bars) and GL (gray trace) are shown.

Pairwise analysis of simultaneously imaged boutons revealed low spontaneous correlations (average similarity = 0.06 ± 0.0003, N = 80,104 bouton pairs; Figure S7E), as well as rich local diversity in response across odors (average similarity = 0.11 ± 0.001, N = 117,352 pairs; Figures 4A and 4C). We observed a small excess of similarly responding boutons within 20 μm separation (Figure 4C; see Experimental Procedures), which can be explained by local enrichment in boutons belonging to the same axon (average distance between boutons anatomically identified on the same axon = 19.5 ± 1.6 μm). Beyond this small excess, no spatial order was apparent in bouton responses within the imaged field of view, implying that nearby boutons were as diverse in their responses as far apart ones (<150 μm, Figure 4C).

Are corticalbulbar feedback responses in the superficial layer organized according to the modular architecture of glomeruli? Within an example field of view, we found that nearby boutons may have very different odor response tuning. Indeed, pairwise comparisons of spontaneous activity (~63,500 pairs, N = 10 FOVs, 6 mice) and odor response spectra (~27,500 pairs, N = 6 fields of view, 4 mice) of bouton pairs showed low correlation across boutons in close proximity of each other, as well as across different fields of view (<150 μm separation, average spontaneous similarity = 0.04 ± 0.0003, average odor similarity = 0.06 ± 0.001; Figures 4B and 4D; Figure S7F). Similar to the GCL, beyond a small excess of similar boutons within 20 μm separation, no obvious spatial organization was observed. Our results suggest that cortical feedback is distributed, locally heterogeneous, and matches the functional diversity observed for example in the responses of some of its potential GC targets (H.C. and D.F.A, unpublished data). These findings contrast previous spatial functionally tuned models of the OB (Johnson and Leon, 2007; Sallaz and Jourdan, 1993; Uchida et al., 2000; Willhite et al., 2006) and are consistent with recent reports of local diversity of glomerular inputs (Ma et al., 2012; Soucy et al., 2009).

We identified two distinct feedback bouton types, strikingly different in the polarity of their odor responses. We set to investigate whether they represent independent channels conveying information from the cortex to the sensory periphery or are redundant in the nature of their odor representations. Within each field of view, for each odor, we assembled a response vector containing the response amplitudes (average dF/F) of all anatomically selected boutons (see Experimental Procedures). We computed the pairwise odor similarity for stimuli within our panel in terms of overlap in their response vectors considering

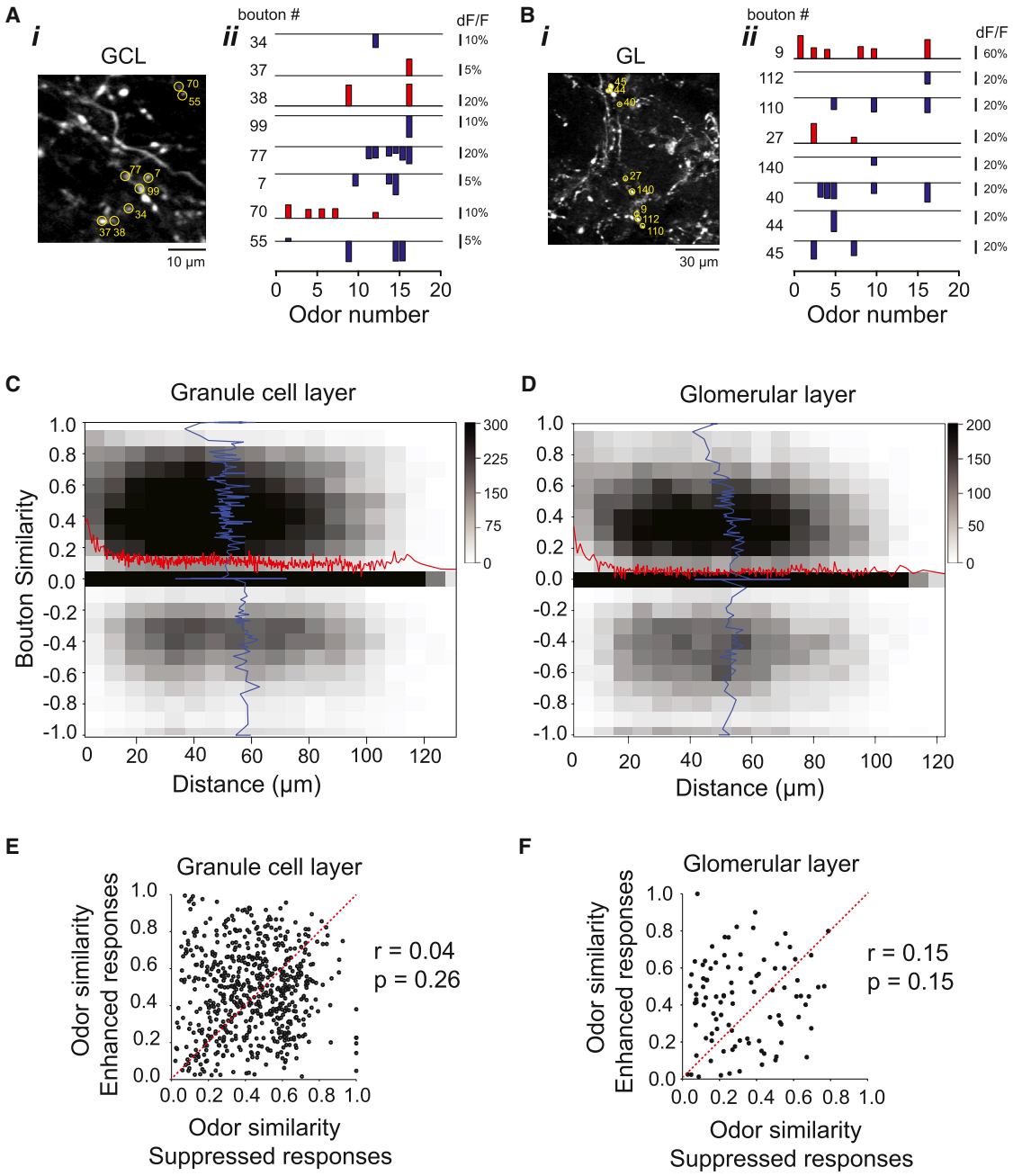

Figure 4. Cortical Feedback Representations Are Locally Diverse

(A and B) Left: example fields of view ~250 µm (A) and ~80 µm (B) from OB surface of GCaMP5-labeled cortical feedback axons and boutons in an awake head-fixed mouse; center: odor response spectra (ORS) of eight example boutons marked in the fluorescence image.

(C and D) Two-dimensional histogram of pairwise correlations between ORS (Odor Set A, Table S1) of individual boutons in the granule cell layer (C) and glomerular layer (D) versus their physical separation. Red, average similarity (pairwise correlation) across different inter-bouton distances; blue, average inter-bouton distance across all similarity values of bouton pairs; grayscale, number of pairs per bin.

(E and F) Odor similarity in terms of only enhanced versus only suppressed bouton responses in the granule cell (E) (r = 0.04) and glomerular layers (F) (r = 0.15); numbers indicate the Pearson's linear correlation coefficient (r) and the associated p values, calculated using a paired t test.

either enhanced responses, or suppressed responses only, respectively. If the average similarity value for an odor pair obtained using the enhanced responses only is predictive of the corresponding value calculated using suppressed responses, then plotting them against each other should result in a cloud of points distributed along a line, with the amplitude and diversity of residuals indicating deviations from this scenario. In both GCL and GL, we did not observe significant correlations between the

two representations (for GCL, r = 0.04 p = 0.27, N = 615 odor pairs; for GL, r = 0.15, p = 0.15, N = 99 odor pairs, t test; Figures 4E and 4F). We computed the mutual information between the similarity in odor representations given by enhanced and suppressed boutons (see Experimental Procedures). We found no significant interdependence between the enhanced and suppressed odor representations in the GL (0.68 bits versus 0.76 ± 0.1 SD bits, shuffled control, p = 0.9), and only small (but statistically significant compared to shuffled control) dependence in GCL (0.21 bits versus 0.16 ± 0.01 SD bits, p < 0.01). Thus, the enhanced and suppressed boutons may represent two distinct piriform cortex output channels, which are relayed back to the sensory periphery.

Cortical Feedback Sparsens Odor Representations and Decorrelates Mitral, but Not Tufted Cell Responses

How does corticalbulbar feedback influence OB output? Our experiments indicate that odors enhance and suppress cortical feedback to the bulb. Hence, in principle, cortical feedback can either inhibit or disinhibit MT cells, via differential regulation of interneuron activity. Therefore, to directly determine the contribution of cortical feedback in shaping MT cell odor responses, we turned to loss-of-function manipulations via pharmacological suppression of activity in the APC. Cortical activity was suppressed by injection of the $GABA_A$ receptor agonist muscimol (fluorescent or non-fluorescent, see Experimental Procedures) through chronically implanted cannulae into the APC (for fluorescent muscimol, ~1 mm A-P and ~0.5 mm M-L, size bolus, N = 3 mice; Figures S5A–S5C) resulting in complete silencing of bouton odor responses (Figures S5D–S5F).

We analyzed the effects of cortical silencing on the activity of mitral (MC) and tufted cells (TC) using multiphoton imaging of GCaMP3.0 signals. We used genetically engineered *TBET*-Cre mice crossed to a GCaMP3.0 reporter line (AI38, Allen Brain Institute; Zariwala et al., 2012) to ensure spatially homogeneous expression of the calcium sensor in MT cells (Haddad et al., 2013). Mitral cells were differentially identified from tufted cells by their denser packing, larger soma size and depth from surface (Figure 5A versus 6A). We observed an increase in the amplitude of response, as well as in the number of odor-responding mitral cells (Figures 5A–5E; Figures S8A and S8B; Movie S4), accompanied by a significant loss of odor selectivity upon muscimol injection (average number of odor responses per cell = 8.37 ± 0.35 pre-muscimol versus 13.92 ± 0.49 post-muscimol, N = 465 MCs, 6 hemibulbs, Wilcoxon signed-rank test, p < 0.001; Figure 5F). We verified that saline injections did not change mitral cell responses (average number of odor responses per cell = 7.32 ± 0.41 pre-saline versus 6.99 ± 0.35, post-saline N = 333 cells, 4 hemi-bulbs, Wilcoxon signed-rank test, p = 0.12; Figure 5D; Figure S8D). A similar trend was observed in average lifetime sparseness quantifications (Figure 5G; Figure S8F).

Consistent with previous reports (Nagayama et al., 2004), we found that tufted cells were more responsive than mitral cells for a given panel of odors, both in amplitude and number of odor responses per cell (Figures 6A–6C). Suppression of APC activity had substantially milder effects on the amplitude and number of responsive TCs (Figures 6D and 6E). In comparison to the effect on MCs, muscimol injection did not significantly alter the number of odor responses for a given TC (average number of odor responses per cell = 15.03 ± 0.49 pre-muscimol versus 14.59 ± 0.51 post-muscimol, N = 309 cells, 5 hemibulbs, Wilcoxon signed-rank test, p = 1; Figure 6F; Movie S5) and only mildly affected TC lifetime sparseness (Figure 6G). No obvious changes were observed in saline injected controls (average number of odor responses per cell = 17.40 ± 0.52 pre-saline versus 15.63 ± 0.51 post-saline, N = 233 cells, 4 hemi-bulbs, Wilcoxon signed-rank test, p = 1; Figures S8E and S8G).

To quantify the effect of APC silencing on mitral and tufted response amplitude, we calculated for each cell the signed Euclidean distance from the diagonal unity line when plotting its response "post" versus "pre" muscimol injection. Increase in response amplitude post-injection will result in values greater than zero (Figures 5E and 6E, see Experimental Procedures). Silencing APC resulted in more robust potentiation of MC versus TC response amplitudes (average distance for MCs = 0.034 ± 0.0008, N = 7,528 odor-cell pairs versus = −0.006 ± 0.002, N = 5,662 odor-TC cell pairs, Wilcoxon rank-sum test, p < 0.001, Figures 5E, 6E, 6H, and 6I). These differential effects between mitral and tufted cells were also reflected in a positive shift in a change index (CI, see Experimental Procedures) calculated to quantify the modulation of response amplitude (average CI for MCs = 0.26 ± 0.008, N = 7,538 odor-cell pairs versus 0.02 ± 0.004, N = 5,662 odor-TC cell pairs, Wilcoxon rank-sum test, p < 0.001).

We analyzed the effects of cortical suppression on the mitral and tufted cell population odor representations (Figure 7A). Muscimol injection significantly increased pairwise similarity (correlation) of odor response spectra (ORS) of simultaneously imaged mitral cells (calculated for signals averaged across repeats), compared to pre-muscimol baseline (average MC similarity = 0.18 ± 0.002, pre-muscimol versus 0.49 ± 0.002, post-muscimol, N = 27,391 mitral cell pairs, Wilcoxon signed-rank test, p < 0.001, Figure 7B; Figure S8C). Importantly, this increase in pairwise correlation was significantly higher than a shuffled control (average shuffled MC similarity = 0.36 ± 0.002, Wilcoxon signed-rank test, p = 0; see Experimental Procedures; Figure S8H) and thus could not simply be explained by increases in the mitral cell odor response amplitude. No significant increase in MC pairwise similarity was observed in saline control experiments (average MC similarity = 0.17 ± 0.002, pre-saline versus 0.15 ± 0.002, post-saline, N = 309 cells, 19,329 MC pairs, 4 hemibulbs, Wilcoxon signed-rank test, p = 1). In contrast, we did not observe any significant change in the pairwise cell ORS similarity across TCs post muscimol injection (average TC similarity = 0.46 ± 0.002, pre-muscimol versus 0.46 ± 0.002, post-muscimol, N = 309 cells, 11,522 TC pairs, 5 hemibulbs, Wilcoxon signed-rank test, p = 0.25; Figure 7C; Figure S8J). Further, scaling down the "post-muscimol" response magnitude by a constant factor ("downscaled muscimol") to match the "pre-muscimol" mean response amplitude did not lead to significant correlation change when compared to the "post-muscimol" condition for neither MCs nor TCs (Figures S8L and S8M).

The higher-odor sensitivity and denser responses in TCs suggest that neuronal representations would be harder to separate on the basis of odor identity when considering TC as opposed to MC population odor responses. Indeed, a pairwise odor correlation analysis (see Experimental Procedures) indicated that

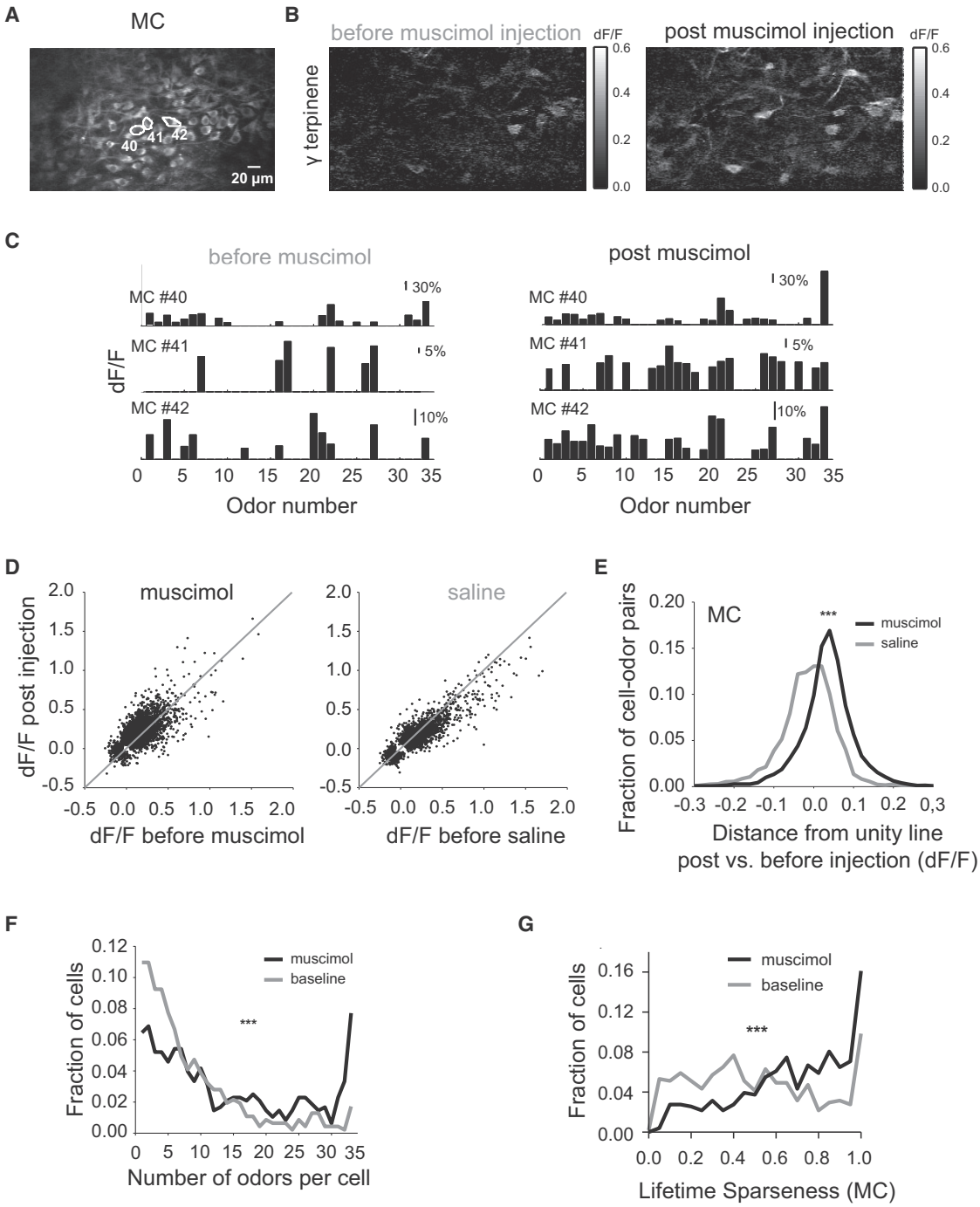

Figure 5. Suppression of APC Activity Increases Mitral Cell Responsiveness

(A) Average resting fluorescence of an example field of view in the mitral cell layer (~220 µm from surface).

(B) Ratio image (dF/F) showing average fluorescence change in response to γ terpinene in the field of view shown in (A) before (left) and after (right) muscimol injection.

(C) Example ORS (Odor Set B, Table S1) of three mitral cell bodies outlined in (A) before (left) and after (right) muscimol injection; each bar indicates the average response amplitude (dF/F) to a given odor in the panel.

(D) Scatter plots showing the odor induced change in mitral cell body fluorescence (dF/F) before and after muscimol (left) and respectively saline injection (right); each dot indicates the response of a cell to a given odor (cell-odor pair) before versus after injection; only cell-odor pairs that were detected as significant in at least one of the two conditions are shown; gray line marks slope of 1.

(legend continued on next page)

TC odor representations (Figure 7A) are more similar across odor stimuli compared to corresponding MC representations (average MC odor similarity = 0.26 ± 0.009 versus 0.49 ± 0.005, N = 528 odor pairs for TC, 10 hemibulbs for MC and 9 hemibulbs for TC, Wilcoxon rank-sum test, $p < 0.001$; see Experimental Procedures; Figures 7D and 7E). In our experiments, more MCs than TCs were imaged simultaneously in a given field of view, which could account in principle for the lower odor similarity in the mitral cells population responses. However, pooling random subsets of cells per field of view, such as to obtain matching number of mitral and tufted cells for computing the odor similarity, reached the same conclusion as above (see Experimental Procedures; Figure S8N). APC silencing resulted in a significant increase in odor similarity in the MC population representations (average MC odor similarity = 0.29 ± 0.01 pre-muscimol versus 0.45 ± 0.01 post-muscimol, N = 528 odor pairs, 6 hemibulbs, Wilcoxon rank-sum test, $p < 0.001$; see Experimental Procedures; Figure 7F; Figure S8I). In contrast, APC silencing had significantly milder effect on the TC odor representations (average TC odor similarity = 0.49 ± 0.005 pre-muscimol versus 0.53 ± 0.003 post-muscimol, N = 528 odor pairs, 5 hemibulbs, Wilcoxon rank-sum test, $p < 0.001$; Figure 7G; Figure S8K). Interestingly, suppression of APC activity brought the odor similarity, as well as pairwise ORS similarity computed for MCs post-muscimol in the range of TC baseline (pre-muscimol) representations. No significant increase in odor similarity in the MC population responses was observed in saline control experiments (average MC odor similarity = 0.20 ± 0.006, pre-saline versus 0.20 ± 0.005, post-saline, N = 528 odor pairs, 4 hemibulbs, Wilcoxon signed-rank test, $p = 0.99$).

Taken together, our results show the existence of specific cortical feedback regulation of the odor representations of mitral versus tufted cells in awake mice. This form of top-down control differentially decorrelates mitral, but not tufted cell population responses, thus potentially enabling odor separation in subsequent olfactory areas.

DISCUSSION

We characterized the dynamics of corticalbulbar feedback projections in awake head-fixed mice across different bulb layers using multiphoton microscopy. Our results indicate that cortical feedback is odor specific, sparse, and layer selective and is routed via two distinct types of boutons which respond mostly with enhancement or suppression of baseline activity (Figures 1, 2, and 3). Feedback representations were locally diverse and often long lasting (Figures 2 and 4). Suppression of these feedback signals via pharmacological silencing of the piriform cortex differentially modulated the OB output, resulting in decreased odor separation across populations of mitral cells, but not tufted cells (Figures 5, 6, and 7).

Corticalbulbar Feedback Is Routed through Distinct Channels of Enhanced and Suppressed Boutons

Previous work in the APC has described spatially distributed and sparse odor responses (Miura et al., 2012; Poo and Isaacson, 2009; Stettler and Axel, 2009; Zhan and Luo, 2010). A study using intracellular recordings in APC of awake mice has reported equal distribution of sparse (responsive to 1 in 20 stimuli, ~50%) and broadly tuned (responding to half or more of sampled stimuli, ~50%) pyramidal cells. The broadly tuned cells were either predominantly excited (25%) or inhibited (25%) by odorants (Zhan and Luo, 2010). Our results show that responses of cortical boutons that project to the OB are largely sparse and odor selective (Figure 1), broadly tuned boutons representing only a small minority (Figure 1I; Figures S2G and S2H). Further, irrespective of their tuning (lifetime sparseness), individual boutons fall into distinct types of "enhanced" and "suppressed" boutons based on their response mode. The differences in broadness of tuning between our observations and APC recordings may reflect anatomical biases in corticalbulbar projection patterns. Functional specificity in feedback projections emerging from primary cortical areas has been reported in the visual and somatosensory systems (Glickfeld et al., 2013; Jarosiewicz et al., 2012; Sato and Svoboda, 2010; Vélez-Fort et al., 2014) and may represent a general feature across sensory modalities.

The functional dichotomy between enhanced and suppressed boutons segregated along axons and could not be explained by imaging artifacts, as indicated by electrical stimulation experiments (Figures S4A–S4C). Our finding is consistent with the existence of different populations of corticalbulbar projecting neurons that respond to odors mostly via enhancement or mostly through suppression. The dichotomy may arise from recurrent excitatory-inhibitory interactions within the APC itself (Franks et al., 2011; Suzuki and Bekkers, 2011; Zhan and Luo, 2010), via presynaptic modulation of cortical feedback fibers in the OB, or both. These models necessitate specific targeting of individual pyramidal neurons/fibers by regulatory circuits and our approach does not distinguish between them. Screening genetically identified classes of APC pyramidal neurons using intersectional strategies (Fenno et al., 2014) in future studies will provide insight into the underlying substrates and the differential effects of these feedback inputs on their OB targets.

Top-down cortical input to the bulb via distinct channels of enhanced and suppressed boutons may be key to increasing the flexibility of feedback action. In one scenario, differential enhancement and suppression may allow feedback to gate

(E) Summary histogram showing change in odor-evoked mitral cells responses upon muscimol (black) and saline (gray) injections compared to pre-injection baseline; the change for each mitral cell odor response (each dot in D is quantified as the Euclidian distance from the diagonal unity line; gray line indicating slope of 1).

(F) Histogram of the number of odors individual mitral cells responded to before (gray trace) and after (black trace) muscimol injection.

(G) Histogram of lifetime sparseness values for individual mitral cells before (gray trace) and after (black trace) muscimol injection (average lifetime sparseness = 0.68 ± 0.01 pre-muscimol versus 0.50 ± 0.01 post-muscimol, N = 509 MCs, 6 hemibulbs, Wilcoxon signed-rank test, $p < 0.001$); *** indicates significance level ($p < 0.001$, Wilcoxon signed-rank test).

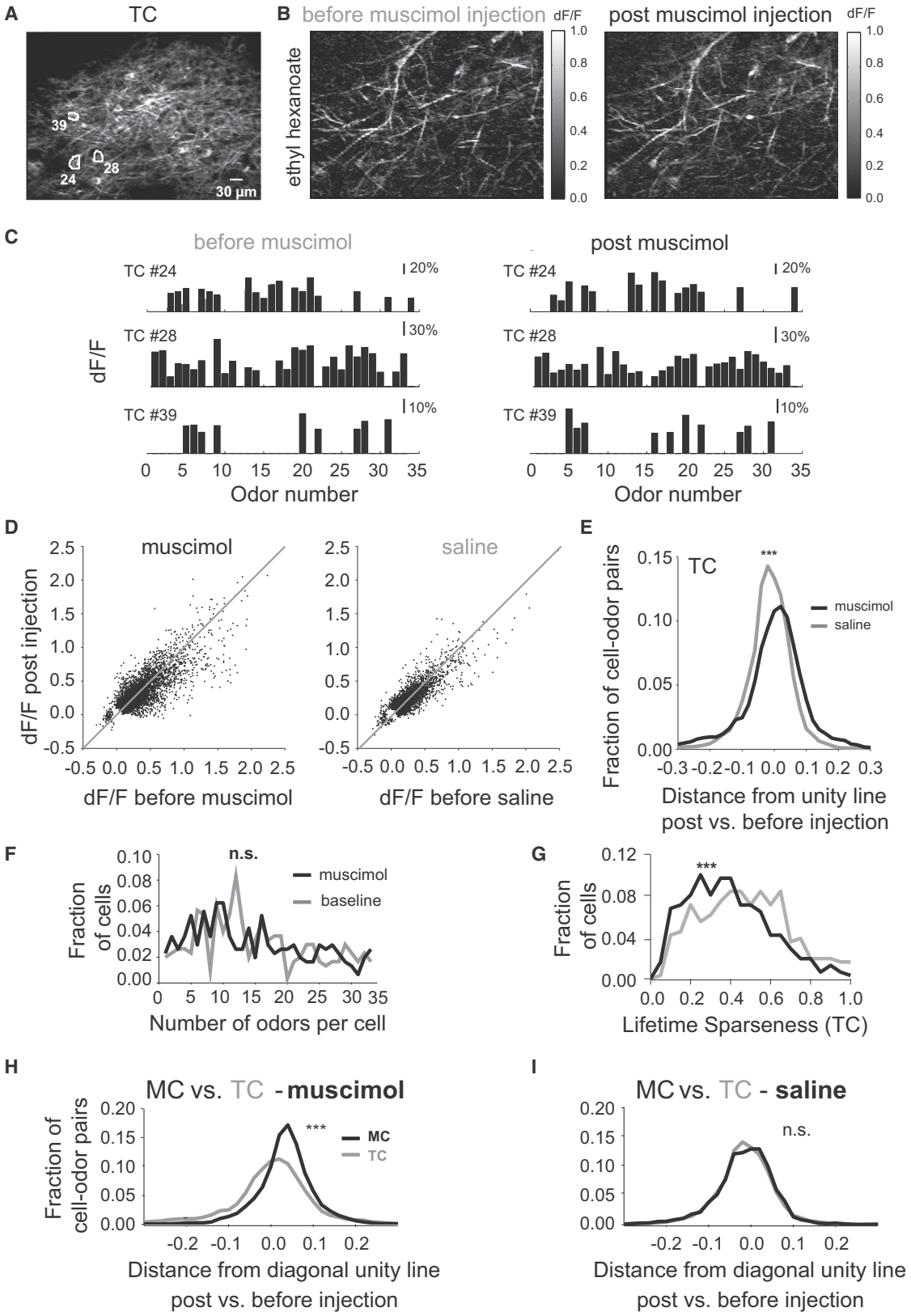

(legend on next page)

specific subsets of OB interneurons and enhance discriminability of behaviorally relevant odors in a context-specific manner.

Cortical Feedback Responses Outlast Odor Stimuli and Are Locally Diverse

We found that feedback responses, especially in the suppressed boutons, often lingered for seconds, long after the end of stimulus presentation (Figure 2; Figure S7). These lasting signals could not simply be explained by slow calcium (reporter) dynamics or motion artifacts, as they were accompanied in the same field of view and same trial by transient responses in neighboring boutons and were preceded in the same boutons by fast spontaneous events during baseline period (Figures 1E and 3B). Also, electrical stimulation experiments demonstrated fast GCaMP5 dynamics (Figures S5G, S5J, and S5K). Persistent feedback responses have also been reported in other brain areas (Petreanu et al., 2012) and may constitute a short-term memory trace that binds recently elicited activity patterns in the APC to ongoing sensory inputs in the OB.

Importantly, responses of corticalbulbar feedback boutons were locally diverse, lacking apparent spatial modular organization both in the glomerular and granule cell layers (Figure 4). This is consistent with recent reports documenting the non-chemotopic organization and functional diversity of the bulbar circuitry (Soucy et al., 2009). Locally heterogeneous feedback inputs together with the long-lasting nature of the responses may allow individual bulbar neurons to integrate olfactory inputs both across a large space of neuronal representations, as well as in time, which are basic ingredients for reconstructing odor identity during active exploration.

Differential Decorrelation of Mitral but Not Tufted Cell Odor Representations by Cortical Feedback

The OB output is relayed to downstream areas via mitral and tufted cells. These two populations differ in anatomical location, response properties and projection patterns (Fukunaga et al., 2012; Igarashi et al., 2012; Nagayama et al., 2004, 2010) and may perform different functions: aiding odor detection versus identification. Suppression of cortical activity had significantly different impact on mitral versus tufted cells (Figures 5, 6, and 7). This may partly arise from the differences observed in cortical feedback responses across the superficial and deep bulb layers (Figure 3). In the absence of feedback, we observed an increase in the similarity of mitral cell odor responses across the population (Figure 7). In contrast, pairwise response similarity across tufted cells showed no significant change. As a consequence, mitral cell population representations of different odors became more similar, suggesting a substantial loss in odor separability for downstream decoder circuits in the absence of corticalbulbar feedback.

Tufted cells intrinsically show higher excitability (shorter latency and stronger response amplitudes), stronger feedforward evoked excitation (Burton and Urban, 2014), and similarity in the odor responses compared to mitral cells. Tufted cells project in high numbers to the AON and olfactory tubercle and could also be differentially modulated by feedback originating from more anterior areas, such as the AON, and to lesser degree from the piriform cortex.

Our results suggest that, in addition to intrinsic biophysical and local connectivity differences between mitral and tufted cells, top-down cortical feedback is an essential ingredient for keeping these two OB output streams distinct from each other.

Decorrelation of ensemble neuronal responses in early sensory circuits has been proposed as a mechanism for separation of similar input patterns by downstream circuits (Laurent, 2002; Vinje and Gallant, 2000; Wiechert et al., 2010). The increased mitral cell correlations in the absence of cortical feedback could not be explained by an increase in mitral cell response amplitude (gain), as indicated by odor identity shuffling controls (Figure S8). Thus, the sparse and distributed cortical feedback does not simply downscale network activity in an unspecific manner, but helps redistribute activity across mitral cells and decorrelates their response patterns to aid odor separation. Our data are consistent with the view that cortical feedback acts specifically via interneurons in the OB, such as to sparsen odor representations at the level of MCs. Future experiments involving faster and

Figure 6. Suppression of APC Activity Only Mildly Alters Tufted Cells Responses

(A) Average resting fluorescence of an example field of view containing tufted cell bodies and dendrites in the external plexiform layer (~140 μm from surface).

(B) Ratio image (dF/F) showing average fluorescence change in response to ethyl hexanoate in the field of view shown in (A) before (left) and after (right) muscimol injection.

(C) Example ORS (Odor Set B, Table S1) of three tufted cell bodies outlined in (E) before (left) and after (right) muscimol injection.

(D) Scatterplots showing the odor-induced change in tufted cell body fluorescence (dF/F) before and after muscimol (left) and respectively saline injection (right); each dot indicates the response of a given cell to a given odor (cell-odor pair) before versus after injection; only cell-odor pairs that were detected as significant in at least one of the two conditions are shown; gray line marks slope of 1.

(E) Summary histogram showing change in odor-evoked tufted cell responses upon muscimol (black) and saline (gray) injections compared to pre-injection baseline; the change for each mitral cell odor response (each dot in D is quantified as the Euclidian distance from the diagonal; gray line indicating slope of 1).

(F) Histogram of the number of odors individual tufted cells responded to before (gray trace) and after (black trace) muscimol injection); Odor Set B, Table S1; n.s. indicates significance level ($p = 1$, Wilcoxon signed-rank test).

(G) Histogram of lifetime sparseness values for individual tufted cells before (gray) and after (black) muscimol injection (average lifetime sparseness = 0.47 ± 0.01 pre-muscimol versus 0.39 ± 0.01 post-muscimol, N = 308 TCs, 5 hemibulbs, Wilcoxon signed-rank test, $p < 0.001$); Odor Set B, Table S1; *** indicates significance level ($p < 0.001$, Wilcoxon signed-rank test).

(H and I) Summary histograms showing change in odor evoked mitral cell (black) and tufted cell (gray) responses upon muscimol (average distance for MCs = 0.034 ± 0.001, N = 7,538 odor-cell pairs versus average distance for TCs = −0.006 ± 0.002, N = 5,662 odor-cell pairs, Wilcoxon rank-sum test, $p < 0.001$) (H) and saline (average distance for MCs = −0.017 ± 0.001, N = 4,719 odor-cell pairs versus average distance for TCs = −0.0157 ± 0.001, N = 3,047 odor-cell pairs, Wilcoxon rank-sum test, $p = 0.56$) (I) injections compared to pre-injection baseline; the change for each cell odor response (each dot in Figures 5D and 6D) is quantified as the Euclidian distance from the diagonal (dotted line indicating slope of 1); *** indicates significance level ($p < 0.001$, Wilcoxon signed-rank test); n.s. indicates $p > 0.05$.

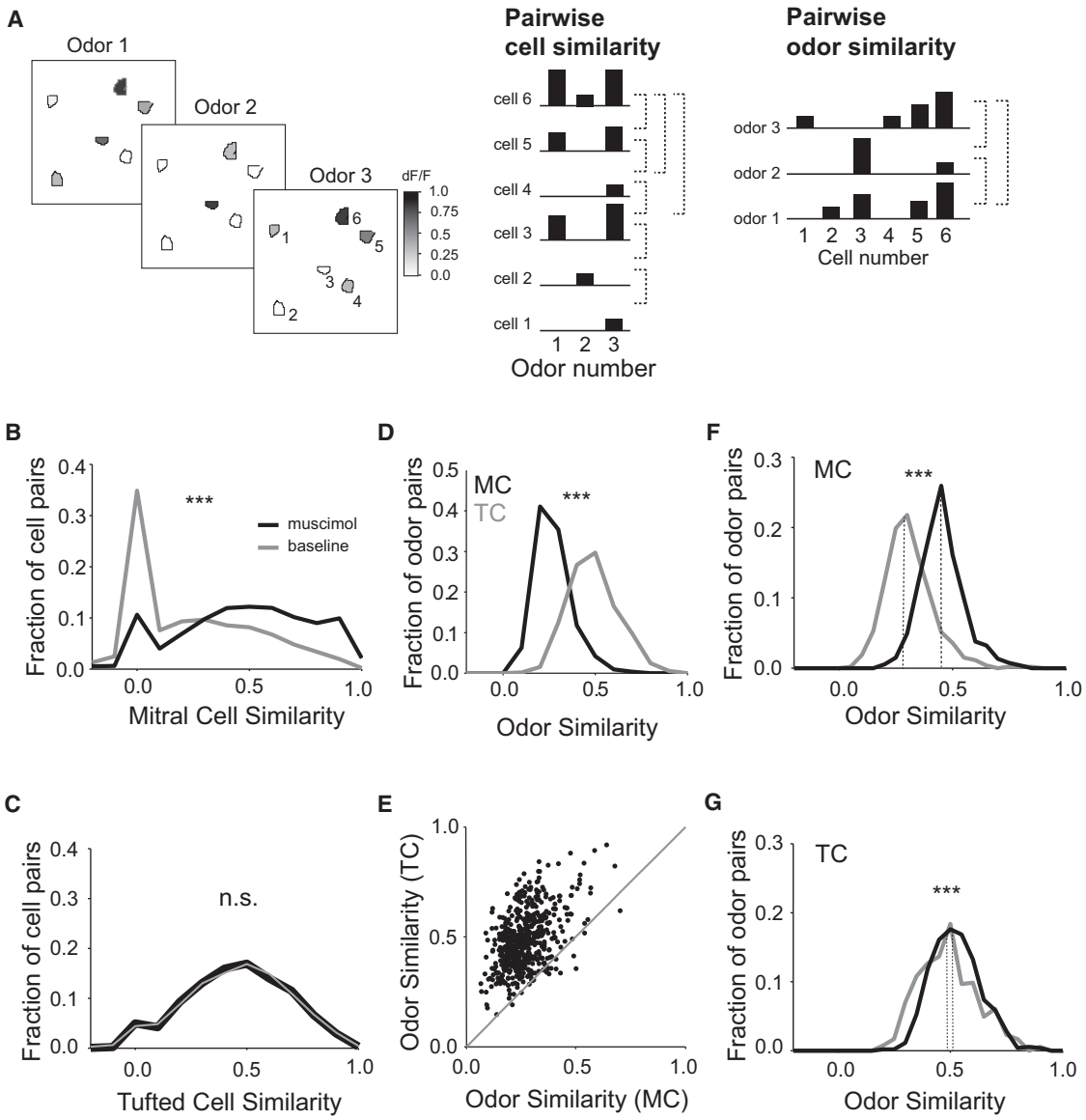

Figure 7. Suppression of APC Activity Decorrelates Mitral, but Not Tufted Cell, Odor Representations

(A) Schematic exemplifying pairwise cell similarity and odor similarity calculations for a given field of view; left: cartoon showing responses of six identified ROIs (black outlines) within a given field of view across three odors; colors indicate the average response amplitude (dF/F) for each ROI; center: an ORS is calculated for each ROI (cell) as the vector containing the average dF/F for each odor; pairwise cell similarity is calculated as the uncentered correlation between the ORS vectors for each pair of cells (indicated by dotted lines); right: a cell response spectrum (CRS) is calculated for each odor as the vector containing the average dF/F for each cell upon presentation of the given odor; pairwise odor similarity is calculated as the uncentered correlation between the CRS vectors for each pair of odors; Odor Set B, Table S1 used for (B)–(G).

(B) Histogram of pairwise cell similarity of mitral cells before (gray, baseline) and after (black) muscimol injection; Odor Set B, Table S1.

(C) Histogram of pairwise cell similarity of tufted cells before (gray, baseline) and after (black) muscimol injection; n.s. indicates significance level ($p = 0.25$, Wilcoxon signed-rank test).

(D) Histogram of pairwise odor similarity of mitral cells (black, MC) and tufted cells (gray, TC) before muscimol injection.

(E) Scatterplot of averaged pairwise odor similarity of mitral versus tufted cells before muscimol injection; each dot represents the comparison of average similarity scores for a given odor pair obtained from mitral and tufted cells odor representations across all sampled fields of view.

(F) Histogram of pairwise odor similarity of mitral cells responses before (gray) and after (black) muscimol injection; dotted lines indicate the median.

(G) Histogram of pairwise odor similarity of tufted cells responses before (gray) and after (black) muscimol injection; *** indicates significance level ($p < 0.001$, Wilcoxon signed-rank test); dotted lines indicate the median.

reversible methods (Boyd et al., 2012; Dhawale et al., 2010; Markopoulos et al., 2012) of suppressing activity, locally applicable in the OB, will help understand how the decorrelation of mitral cell outputs evolves over time and how it impacts odor discrimination speed and accuracy in behaving animals.

Our experiments characterizing the functional properties and spatial-temporal organization of corticalbulbar projections are a starting point in understanding how top-down signals originating in the piriform cortex guide olfactory processing. Monitoring the dynamics of corticalbulbar feedback and the consequences of targeted suppression of feedback fibers in animals analyzing varying odor signals in rich olfactory environments will advance our understanding of cortical feedback function during behavior.

EXPERIMENTAL PROCEDURES

All animal procedures conformed to NIH guidelines and were approved by Cold Spring Harbor Laboratory Institutional Animal Care and Use Committee. Detailed methods are available as Supplemental Experimental Procedures. To express GCaMP5 in corticalbulbar axons, we anesthetized adult mice with ketamine/xylazine and injected them with a cocktail of AAV2.9 *Synapsin-Cre* and AAV2.9 *EF1-DIO-GCaMP5* in the APC at least 2 weeks before imaging. To gain optical access to the OB, we anesthetized animals, removed the bone over the bulb, and replaced it by a 3 mm coverslip (CS-3R, Warner Instruments). A titanium headbar was attached to the skull to fixate the animal during the imaging sessions. Mice were imaged using a Chameleon Ultra II Ti:Sapphire femtosecond pulsed laser (Coherent) coupled to a custom built multiphoton microscope.

Odor Delivery

Odors were presented in 4 s pulses, preceded by 10 s baseline and followed by 12 s recovery periods. Inter-trial intervals (ITIs) of at least 30 s were used between recording periods. During each ITI, a high air flow stream (>20 l/min) was pushed through the odor delivery machine to minimize odor contamination across trials. A serial air dilution odor machine was used to deliver odorized air (Odor Set A, Table S1) at 2.5 l/min rate at 0.4% saturated vapor pressure (Figures 1D–1J, 2A, 2B, 2D, 3, and 4). For experiments comparing bouton responses in awake versus anesthetized mice, as well as monitoring the effects of muscimol, a subset of 5 odors was used (acetal, hexanal, ethyl tiglate, ethyl caproate, and isoamyl acetate). A second, oil dilution-based odor machine (1 l/min rate; Dhawale et al., 2010) was used for experiments involving larger odor sets (1:100 mineral oil dilution, Odor Set B, Table S1, for mitral and tufted cell imaging experiments, Figures 5, 6, and 7), and for probing concentrations (Concentration, Table S1, $1{:}10^4$ to 1:10 nominal oil dilutions). Odor output was characterized using a photo-ionization device (Aurora Scientific) and calibrated in terms of concentration in air (Figure S6A). Odors in the panel were chemically diverse and activated glomeruli on the dorsal OB surface.

Data analysis

Image Registration

Images were registered using either the ImageJ plugin TurboReg (Turboreg) or via a previously described method (Guizar-Sicairos et al., 2008). The average registered image for each individual odor presentation was visually inspected to detect slow drifts in the z plane. Such instances were further discarded. ROIs were manually drawn for individual boutons (0.9–3 μm diameter) in ImageJ. For mitral and tufted cells imaging sessions, ROIs were manually selected based on anatomy (baseline average fluorescence). Care was taken to avoid selecting ROIs on cell bodies overlapping with neuropil (M/T lateral dendrites). To detect fast z movement on individual frames, we compared the shapes of each ROI in each frame with their corresponding averaged frames. Frames were a majority of ROIs changed shape were discarded from the analysis.

Spontaneous Activity, Assignment of Boutons, and Signal Detection

To detect spontaneous events, we estimated the distribution of resting fluorescence from the lower half of fluorescence values in the data. A fluorescence increase was called a spontaneous event if it exceeded the 99th percentile of the resting fluorescence. An ROI was considered spontaneously active if it showed at least two spontaneous events during a 3 min window. To determine whether two boutons belonged to the same axon, we visually inspected whether they appeared connected by an axonal segment in the imaged plane (337 "same axon" pairs, 52 axonal segments, and 648 "different axon" bouton pairs).

For each ROI and each odor presentation, the fluorescence signal across time was converted into dF/F values

$$(dF/F)_t = (F_t - F_o)/F_o$$

where, $(dF/F)_t$ is the baseline subtracted, normalized fluorescence at time t; F_t is the instantaneous fluorescence at time t; and, F_o is the median fluorescence value during the initial air period.

Upon odor presentation, axonal boutons, mitral and tufted cells responded by increasing, and decreasing their fluorescence. ROI response to an odor presentation was quantified as the average dF/F over 4 s of odor presentation. To determine significance, we compared the odor evoked normalized fluorescence with values calculated during the air periods preceding all odor presentations in the session. Responses that exceeded the 99.9 percentile were called significantly *enhanced*. Responses that were below the 0.1 percentile were considered significantly *suppressed*. An ROI that showed significant responses to an odor in at least two repeats was considered *responsive* to that odor.

Concentration Invariance

Significance of each ROI for each odor response at each concentration was assessed independently. An ROI was classified as concentration invariant only if it cleared significance at all four concentrations used and the magnitude of responses did not differ across concentrations. To establish whether an ROI showed monotonically increasing or decreasing responses to a given odor across concentrations, its concentration response curve (described above) was fitted with a line and its slope was compared to the distribution of slopes obtained by shuffling the concentration labels. An odor response curve was called monotonically increasing (decreasing) if the slope was larger (smaller) than the 95% (5%) percentile of the slopes of the shuffled distributions.

The Odor Response Spectrum (ORS) for a given ROI was described as the vector of length equally to number of odors used, containing the average responses across trials to each odor. Non-significant odors responses were set to 0. Similarity between the ORS of two ROIs, ORS_i and ORS_j, was defined as the un-centered correlation coefficient (equivalent to cosine of the angle) between the two vectors:

$$similarity = \frac{ORS_i \cdot ORS_j}{\sqrt{(ORS_i \cdot ORS_i)(ORS_j \cdot ORS_j)}}.$$

Similarly, we defined the population response (Cell Response Spectrum [CRS]) to an odor for a given field of view (FOV) as the vector of responses of all ROIs in the FOV responsive to that odor. ROIs with non-significant responses were set to zero. Odor similarity between two population responses was also defined as the un-centered correlation coefficient between the population response vectors.

Distance from diagonal unity line before versus after muscimol or saline injection and a change index (CI) were calculated only for cells that showed a significant response before or after injection. Distance from diagonal unity line was defined as shortest distance (normal) to the identity diagonal line in the scatter plot of odor responses before and after injection. Absolute value of change index (CI_{abs}) was defined as:

$$CI_{abs} = \frac{|Response\ post\ injection - Response\ before\ injection|}{|Response\ post\ injection| + |Response\ before\ injection|}.$$

Sign of distance from diagonal line and CI was positive if:

$$|Response\ post\ injection| \geq |Response\ before\ injection|$$

and negative if:

$$|Response\ post\ injection| < |Response\ before\ injection|.$$

Most mitral and tufted cell GCaMP3 odor responses (> 90%) were positive. Hence, the use of absolute values did not affect our conclusions.

SUPPLEMENTAL INFORMATION

Supplemental Information includes Supplemental Experimental Procedures, eight figures, one table, and five movies and can be found with this article online at http://dx.doi.org/10.1016/j.neuron.2015.05.023.

AUTHOR CONTRIBUTIONS

G.H.O., H.C., and D.F.A. conceptualized the study and contributed to the practical design of experiments and analysis. G.H.O. and H.C. performed OB imaging and APC electrical stimulation and silencing experiments. M.B.D. performed viral injections and immunohistochemistry. G.H.O., H.C., and D.F.A. wrote the manuscript.

ACKNOWLEDGMENTS

We would like to thank P. Gupta for valuable input on manuscript preparation and A. Dăbâcan, A. Banerjee, and members of the D.F.A. laboratory for comments on the manuscript. This study was supported by a Pew Scholarship, Whitehall Fellowship and CSHL startup funds. In memoriam Mihai Pătraşcu.

Received: September 2, 2014
Revised: February 21, 2015
Accepted: May 7, 2015
Published: June 4, 2015

REFERENCES

Akerboom, J., Chen, T.-W., Wardill, T.J., Tian, L., Marvin, J.S., Mutlu, S., Calderón, N.C., Esposti, F., Borghuis, B.G., Sun, X.R., et al. (2012). Optimization of a GCaMP calcium indicator for neural activity imaging. J. Neurosci. *32*, 13819–13840.

Babadi, B., and Sompolinsky, H. (2014). Sparseness and expansion in sensory representations. Neuron *83*, 1213–1226.

Balu, R., Pressler, R.T., and Strowbridge, B.W. (2007). Multiple modes of synaptic excitation of olfactory bulb granule cells. J. Neurosci. *27*, 5621–5632.

Barak, O., Rigotti, M., and Fusi, S. (2013). The sparseness of mixed selectivity neurons controls the generalization-discrimination trade-off. J. Neurosci. *33*, 3844–3856.

Boyd, A.M., Sturgill, J.F., Poo, C., and Isaacson, J.S. (2012). Cortical feedback control of olfactory bulb circuits. Neuron *76*, 1161–1174.

Burton, S.D., and Urban, N.N. (2014). Greater excitability and firing irregularity of tufted cells underlies distinct afferent-evoked activity of olfactory bulb mitral and tufted cells. J. Physiol. *592*, 2097–2118.

Caron, S.J.C., Ruta, V., Abbott, L.F., and Axel, R. (2013). Random convergence of olfactory inputs in the Drosophila mushroom body. Nature *497*, 113–117.

Devore, S., and Linster, C. (2012). Noradrenergic and cholinergic modulation of olfactory bulb sensory processing. Front. Behav. Neurosci. *6*, 52.

Dhawale, A.K., Hagiwara, A., Bhalla, U.S., Murthy, V.N., and Albeanu, D.F. (2010). Non-redundant odor coding by sister mitral cells revealed by light addressable glomeruli in the mouse. Nat. Neurosci. *13*, 1404–1412.

Fenno, L.E., Mattis, J., Ramakrishnan, C., Hyun, M., Lee, S.Y., He, M., Tucciarone, J., Selimbeyoglu, A., Berndt, A., Grosenick, L., et al. (2014). Targeting cells with single vectors using multiple-feature Boolean logic. Nat. Methods *11*, 763–772.

Franks, K.M., Russo, M.J., Sosulski, D.L., Mulligan, A.A., Siegelbaum, S.A., and Axel, R. (2011). Recurrent circuitry dynamically shapes the activation of piriform cortex. Neuron *72*, 49–56.

Fukunaga, I., Berning, M., Kollo, M., Schmaltz, A., and Schaefer, A.T. (2012). Two distinct channels of olfactory bulb output. Neuron *75*, 320–329.

Ghosh, S., Larson, S.D., Hefzi, H., Marnoy, Z., Cutforth, T., Dokka, K., and Baldwin, K.K. (2011). Sensory maps in the olfactory cortex defined by long-range viral tracing of single neurons. Nature *472*, 217–220.

Gilbert, C.D., and Li, W. (2013). Top-down influences on visual processing. Nat. Rev. Neurosci. *14*, 350–363.

Glickfeld, L.L., Andermann, M.L., Bonin, V., and Reid, R.C. (2013). Cortico-cortical projections in mouse visual cortex are functionally target specific. Nat. Neurosci. *16*, 219–226.

Gottfried, J.A. (2010). Central mechanisms of odour object perception. Nat. Rev. Neurosci. *11*, 628–641.

Gray, C.M., and Skinner, J.E. (1988). Centrifugal regulation of neuronal activity in the olfactory bulb of the waking rabbit as revealed by reversible cryogenic blockade. Exp. Brain Res. *69*, 378–386.

Guizar-Sicairos, M., Thurman, S.T., and Fienup, J.R. (2008). Efficient subpixel image registration algorithms. Opt. Lett. *33*, 156–158.

Haberly, L.B. (2001). Parallel-distributed processing in olfactory cortex: new insights from morphological and physiological analysis of neuronal circuitry. Chem. Senses *26*, 551–576.

Haberly, L.B., and Bower, J.M. (1989). Olfactory cortex: model circuit for study of associative memory? Trends Neurosci. *12*, 258–264.

Haddad, R., Lanjuin, A., Madisen, L., Zeng, H., Murthy, V.N., and Uchida, N. (2013). Olfactory cortical neurons read out a relative time code in the olfactory bulb. Nat. Neurosci. *16*, 949–957.

Harris, K.D., and Mrsic-Flogel, T.D. (2013). Cortical connectivity and sensory coding. Nature *503*, 51–58.

Igarashi, K.M., Ieki, N., An, M., Yamaguchi, Y., Nagayama, S., Kobayakawa, K., Kobayakawa, R., Tanifuji, M., Sakano, H., Chen, W.R., and Mori, K. (2012). Parallel mitral and tufted cell pathways route distinct odor information to different targets in the olfactory cortex. J. Neurosci. *32*, 7970–7985.

Jarosiewicz, B., Schummers, J., Malik, W.Q., Brown, E.N., and Sur, M. (2012). Functional biases in visual cortex neurons with identified projections to higher cortical targets. Curr. Biol. *22*, 269–277.

Johnson, B.A., and Leon, M. (2007). Chemotopic odorant coding in a mammalian olfactory system. J. Comp. Neurol. *503*, 1–34.

Kaplan, B.A., and Lansner, A. (2014). A spiking neural network model of self-organized pattern recognition in the early mammalian olfactory system. Front. Neural Circuits *8*, 5.

Laurent, G. (2002). Olfactory network dynamics and the coding of multidimensional signals. Nat. Rev. Neurosci. *3*, 884–895.

Linster, C., and Hasselmo, M.E. (2001). Neuromodulation and the functional dynamics of piriform cortex. Chem. Senses *26*, 585–594.

Ma, L., Qiu, Q., Gradwohl, S., Scott, A., Yu, E.Q., Alexander, R., Wiegraebe, W., and Yu, C.R. (2012). Distributed representation of chemical features and tunotopic organization of glomeruli in the mouse olfactory bulb. Proc. Natl. Acad. Sci. USA *109*, 5481–5486.

Manabe, H., and Mori, K. (2013). Sniff rhythm-paced fast and slow gamma-oscillations in the olfactory bulb: relation to tufted and mitral cells and behavioral states. J. Neurophysiol. *110*, 1593–1599.

Margrie, T.W., Sakmann, B., and Urban, N.N. (2001). Action potential propagation in mitral cell lateral dendrites is decremental and controls recurrent and lateral inhibition in the mammalian olfactory bulb. Proc. Natl. Acad. Sci. USA *98*, 319–324.

Markopoulos, F., Rokni, D., Gire, D.H., and Murthy, V.N. (2012). Functional properties of cortical feedback projections to the olfactory bulb. Neuron *76*, 1175–1188.

Matsutani, S. (2010). Trajectory and terminal distribution of single centrifugal axons from olfactory cortical areas in the rat olfactory bulb. Neuroscience *169*, 436–448.

McCollum, J., Larson, J., Otto, T., Schottler, F., Granger, R., and Lynch, G. (1991). Short-latency single unit processing in olfactory cortex. J. Cogn. Neurosci. *3*, 293–299.

Miura, K., Mainen, Z.F., and Uchida, N. (2012). Odor representations in olfactory cortex: distributed rate coding and decorrelated population activity. Neuron *74*, 1087–1098.

Miyamichi, K., Amat, F., Moussavi, F., Wang, C., Wickersham, I., Wall, N.R., Taniguchi, H., Tasic, B., Huang, Z.J., He, Z., et al. (2011). Cortical representations of olfactory input by trans-synaptic tracing. Nature *472*, 191–196.

Nagayama, S., Takahashi, Y.K., Yoshihara, Y., and Mori, K. (2004). Mitral and tufted cells differ in the decoding manner of odor maps in the rat olfactory bulb. J. Neurophysiol. *91*, 2532–2540.

Nagayama, S., Enerva, A., Fletcher, M.L., Masurkar, A.V., Igarashi, K.M., Mori, K., and Chen, W.R. (2010). Differential axonal projection of mitral and tufted cells in the mouse main olfactory system. Front Neural Circuits *4*, 120.

Nakashima, M., Mori, K., and Takagi, S.F. (1978). Centrifugal influence on olfactory bulb activity in the rabbit. Brain Res. *154*, 301–306.

Nunez-Parra, A., Maurer, R.K., Krahe, K., Smith, R.S., and Araneda, R.C. (2013). Disruption of centrifugal inhibition to olfactory bulb granule cells impairs olfactory discrimination. Proc. Natl. Acad. Sci. USA *110*, 14777–14782.

Oswald, A.-M., and Urban, N.N. (2012). There and back again: the corticobulbar loop. Neuron *76*, 1045–1047.

Otazu, G.H., and Leibold, C. (2011). A corticothalamic circuit model for sound identification in complex scenes. PLoS ONE *6*, e24270.

Petreanu, L., Gutnisky, D.A., Huber, D., Xu, N.L., O'Connor, D.H., Tian, L., Looger, L., and Svoboda, K. (2012). Activity in motor-sensory projections reveals distributed coding in somatosensation. Nature *489*, 299–303.

Petzold, G.C., Hagiwara, A., and Murthy, V.N. (2009). Serotonergic modulation of odor input to the mammalian olfactory bulb. Nat. Neurosci. *12*, 784–791.

Poo, C., and Isaacson, J.S. (2009). Odor representations in olfactory cortex: "sparse" coding, global inhibition, and oscillations. Neuron *62*, 850–861.

Ranade, S.P., and Mainen, Z.F. (2009). Transient firing of dorsal raphe neurons encodes diverse and specific sensory, motor, and reward events. J. Neurophysiol. *102*, 3026–3037.

Rao, R.P., and Ballard, D.H. (1999). Predictive coding in the visual cortex: a functional interpretation of some extra-classical receptive-field effects. Nat. Neurosci. *2*, 79–87.

Rothermel, M., and Wachowiak, M. (2014). Functional imaging of cortical feedback projections to the olfactory bulb. Front. Neural Circuits *8*, 73.

Sallaz, M., and Jourdan, F. (1993). C-fos expression and 2-deoxyglucose uptake in the olfactory bulb of odour-stimulated awake rats. Neuroreport *4*, 55–58.

Sato, T.R., and Svoboda, K. (2010). The functional properties of barrel cortex neurons projecting to the primary motor cortex. J. Neurosci. *30*, 4256–4260.

Shepherd, G.M. (1972). Synaptic organization of the mammalian olfactory bulb. Physiol. Rev. *52*, 864–917.

Shipley, M.T., and Adamek, G.D. (1984). The connections of the mouse olfactory bulb: a study using orthograde and retrograde transport of wheat germ agglutinin conjugated to horseradish peroxidase. Brain Res. Bull. *12*, 669–688.

Sosulski, D.L., Bloom, M.L., Cutforth, T., Axel, R., and Datta, S.R. (2011). Distinct representations of olfactory information in different cortical centres. Nature *472*, 213–216.

Soucy, E.R., Albeanu, D.F., Fantana, A.L., Murthy, V.N., and Meister, M. (2009). Precision and diversity in an odor map on the olfactory bulb. Nat. Neurosci. *12*, 210–220.

Stettler, D.D., and Axel, R. (2009). Representations of odor in the piriform cortex. Neuron *63*, 854–864.

Suzuki, N., and Bekkers, J.M. (2011). Two layers of synaptic processing by principal neurons in piriform cortex. J. Neurosci. *31*, 2156–2166.

Taniguchi, H., He, M., Wu, P., Kim, S., Paik, R., Sugino, K., Kvitsiani, D., Fu, Y., Lu, J., Lin, Y., et al. (2011). A resource of Cre driver lines for genetic targeting of GABAergic neurons in cerebral cortex. Neuron *71*, 995–1013.

Tian, L., Hires, S.A., Mao, T., Huber, D., Chiappe, M.E., Chalasani, S.H., Petreanu, L., Akerboom, J., McKinney, S.A., Schreiter, E.R., et al. (2009). Imaging neural activity in worms, flies and mice with improved GCaMP calcium indicators. Nat. Methods *6*, 875–881.

Tobin, V.A., Hashimoto, H., Wacker, D.W., Takayanagi, Y., Langnaese, K., Caquineau, C., Noack, J., Landgraf, R., Onaka, T., Leng, G., et al. (2010). An intrinsic vasopressin system in the olfactory bulb is involved in social recognition. Nature *464*, 413–417.

Uchida, N., Takahashi, Y.K., Tanifuji, M., and Mori, K. (2000). Odor maps in the mammalian olfactory bulb: domain organization and odorant structural features. Nat. Neurosci. *3*, 1035–1043.

Urban, N.N., and Sakmann, B. (2002). Reciprocal intraglomerular excitation and intra- and interglomerular lateral inhibition between mouse olfactory bulb mitral cells. J. Physiol. *542*, 355–367.

Vélez-Fort, M., Rousseau, C.V., Niedworok, C.J., Wickersham, I.R., Rancz, E.A., Brown, A.P.Y., Strom, M., and Margrie, T.W. (2014). The stimulus selectivity and connectivity of layer six principal cells reveals cortical microcircuits underlying visual processing. Neuron *83*, 1431–1443.

Vickers, N.J. (2000). Mechanisms of animal navigation in odor plumes. Biol. Bull. *198*, 203–212.

Vinje, W.E., and Gallant, J.L. (2000). Sparse coding and decorrelation in primary visual cortex during natural vision. Science *287*, 1273–1276.

Wachowiak, M., Wesson, D.W., Pírez, N., Verhagen, J.V., and Carey, R.M. (2009). Low-level mechanisms for processing odor information in the behaving animal. Ann. N Y Acad. Sci. *1170*, 286–292.

Wiechert, M.T., Judkewitz, B., Riecke, H., and Friedrich, R.W. (2010). Mechanisms of pattern decorrelation by recurrent neuronal circuits. Nat. Neurosci. *13*, 1003–1010.

Willhite, D.C., Nguyen, K.T., Masurkar, A.V., Greer, C.A., Shepherd, G.M., and Chen, W.R. (2006). Viral tracing identifies distributed columnar organization in the olfactory bulb. Proc. Natl. Acad. Sci. USA *103*, 12592–12597.

Wilson, R.I., and Mainen, Z.F. (2006). Early events in olfactory processing. Annu. Rev. Neurosci. *29*, 163–201.

Wilson, D.A., and Sullivan, R.M. (2011). Cortical processing of odor objects. Neuron *72*, 506–519.

Wilson, D.A., Fletcher, M.L., and Sullivan, R.M. (2004). Acetylcholine and olfactory perceptual learning. Learn. Mem. *11*, 28–34.

Zariwala, H.A., Borghuis, B.G., Hoogland, T.M., Madisen, L., Tian, L., De Zeeuw, C.I., Zeng, H., Looger, L.L., Svoboda, K., and Chen, T.-W. (2012). A Cre-dependent GCaMP3 reporter mouse for neuronal imaging in vivo. J. Neurosci. *32*, 3131–3141.

Zhan, C., and Luo, M. (2010). Diverse patterns of odor representation by neurons in the anterior piriform cortex of awake mice. J. Neurosci. *30*, 16662–16672.

Neuron

Supplemental Information

Cortical Feedback Decorrelates Olfactory Bulb Output in Awake Mice

Gonzalo H. Otazu, Hong Goo Chae, Martin B. Davis, and Dinu F. Albeanu

Figure S1

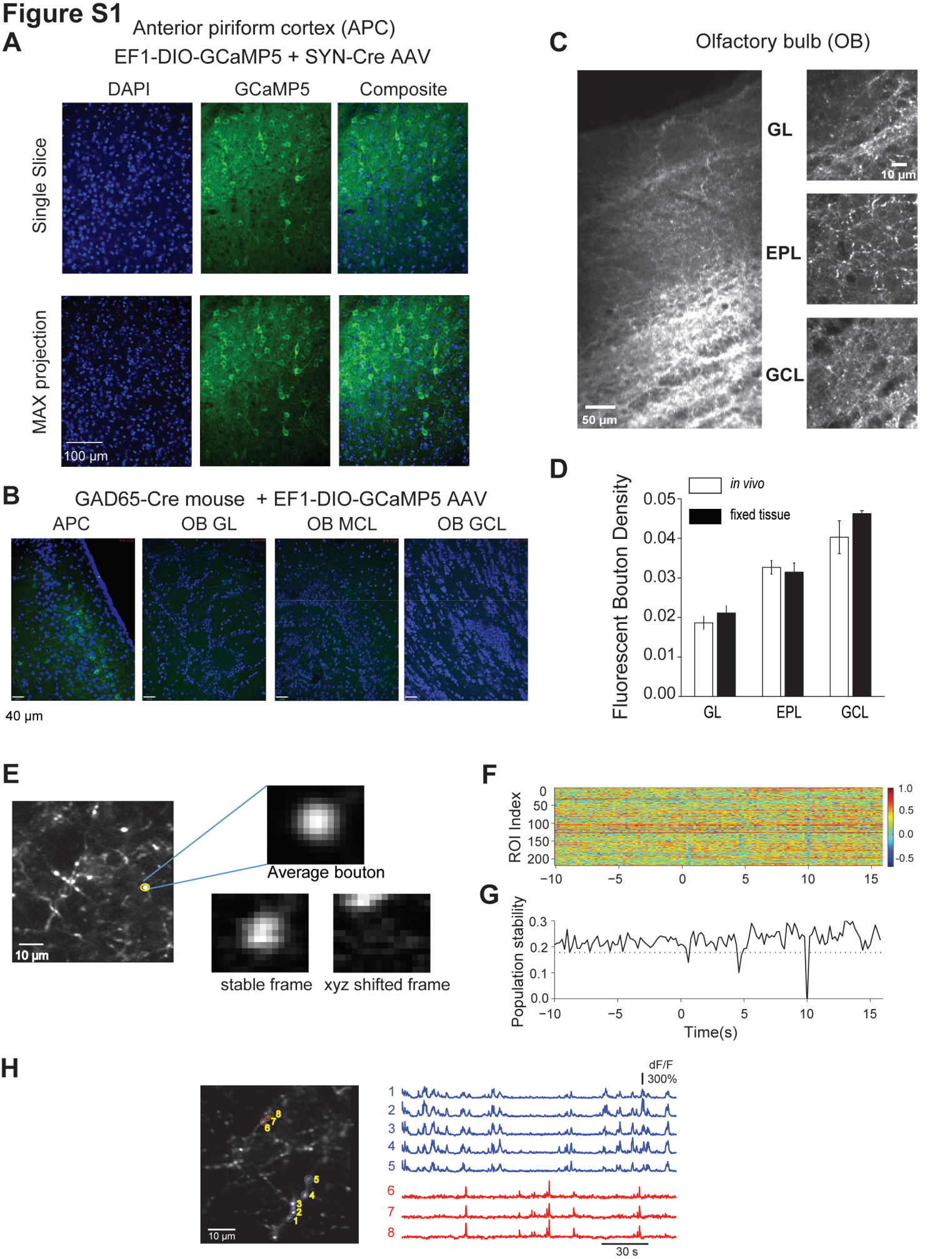
A
Anterior piriform cortex (APC)
EF1-DIO-GCaMP5 + SYN-Cre AAV
DAPI
GCaMP5
Composite
Single Slice
MAX projection
100 µm
B
GAD65-Cre mouse + EF1-DIO-GCaMP5 AAV
APC
OB GL
OB MCL
OB GCL
40 µm
C
Olfactory bulb (OB)
GL
EPL
GCL
50 µm
10 µm
D
Fluorescent Bouton Density
in vivo
fixed tissue
0.05
0.04
0.03
0.02
0.01
0.00
GL
EPL
GCL
E
10 µm
Average bouton
stable frame
xyz shifted frame
F
ROI Index
0
50
100
150
200
−10
−5
0
5
10
15
1.0
0.5
0.0
-0.5
G
Population stability
0.3
0.2
0.1
0.0
−10
−5
0
5
10
15
Time(s)
H
10 µm
dF/F
300%
1
2
3
4
5
6
7
8
30 s

Figure S2

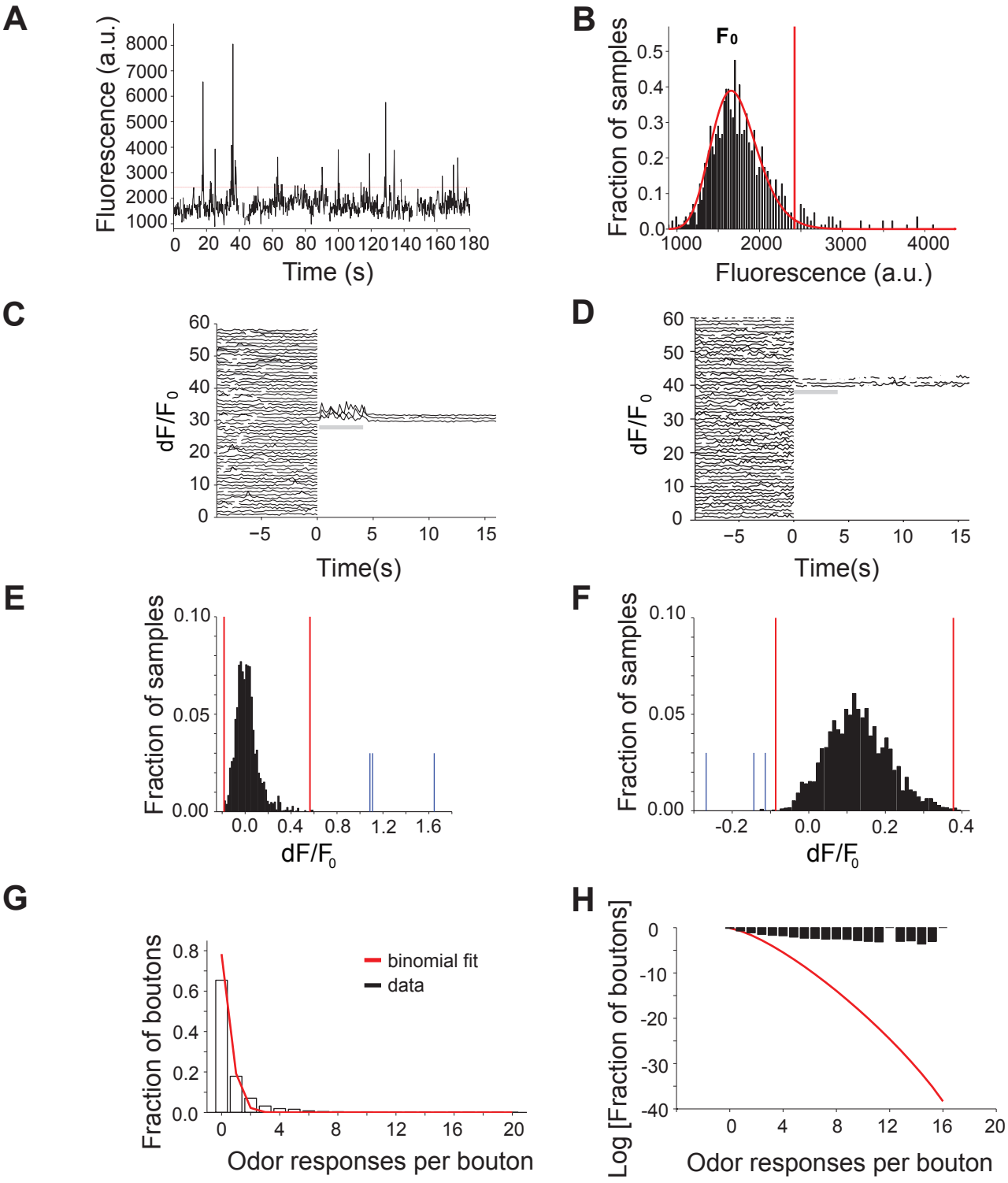
A
Fluorescence (a.u.)
8000
7000
6000
5000
4000
3000
2000
1000
0 20 40 60 80 100 120 140 160 180
Time (s)
B
F0
Fraction of samples
0.5
0.4
0.3
0.2
0.1
0.0
1000 2000 3000 4000
Fluorescence (a.u.)
C
dF/F0
60
50
40
30
20
10
0
−5 0 5 10 15
Time(s)
D
dF/F0
60
50
40
30
20
10
0
−5 0 5 10 15
Time(s)
E
Fraction of samples
0.10
0.05
0.00
0.0 0.4 0.8 1.2 1.6
dF/F0
F
Fraction of samples
0.10
0.05
0.00
-0.2 0.0 0.2 0.4
dF/F0
G
Fraction of boutons
0.8
0.6
0.4
0.2
0.0
0 4 8 12 16 20
Odor responses per bouton
binomial fit
data
H
Log [Fraction of boutons]
0
-10
-20
-30
-40
0 4 8 12 16 20
Odor responses per bouton

Figure S3

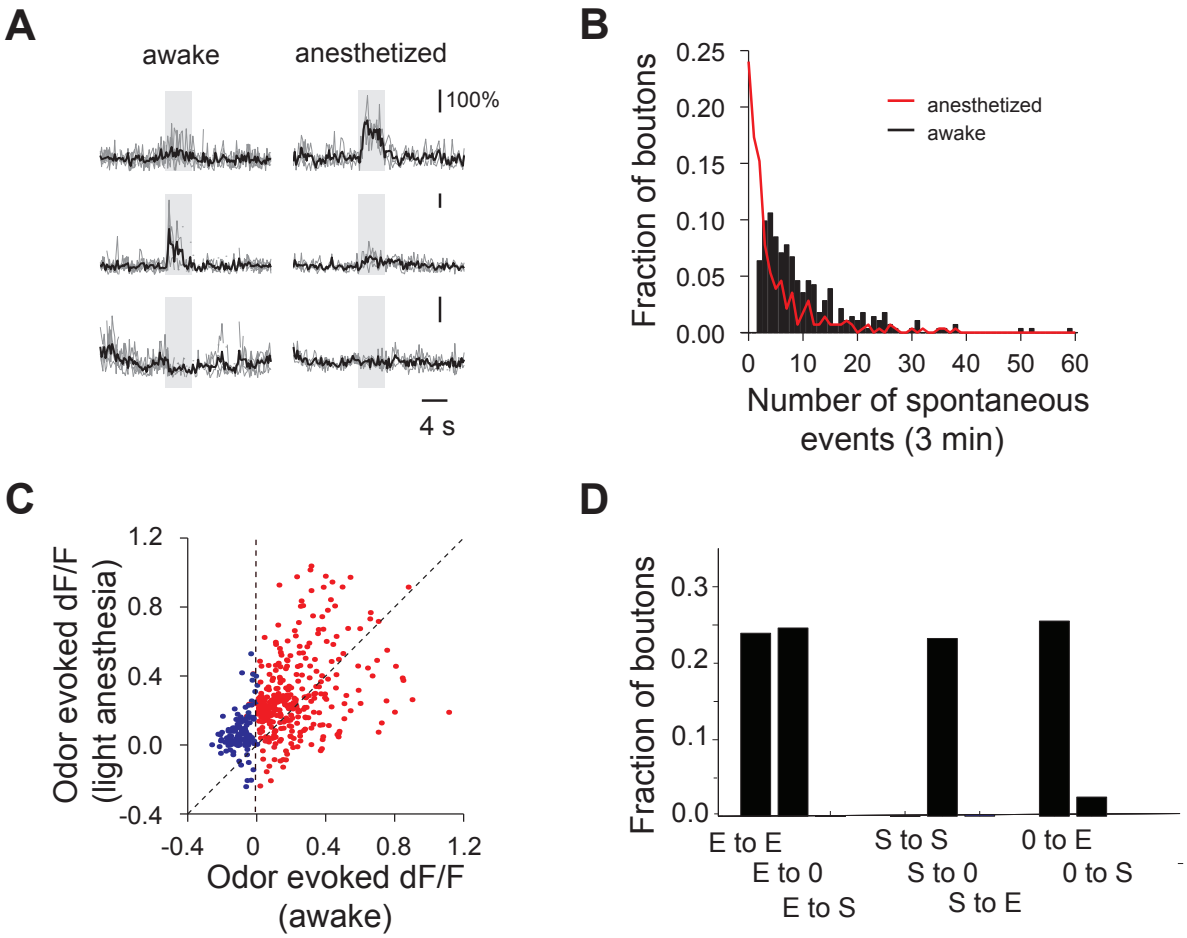
A
awake
anesthetized
100%
4 s
B
Fraction of boutons
0.25
0.20
0.15
0.10
0.05
0.00
anesthetized
awake
0
10
20
30
40
50
60
Number of spontaneous events (3 min)
C
Odor evoked dF/F (light anesthesia)
1.2
0.8
0.4
0.0
-0.4
-0.4
0
0.4
0.8
1.2
Odor evoked dF/F (awake)
D
Fraction of boutons
0.3
0.2
0.1
0.0
E to E
E to 0
E to S
S to S
S to 0
S to E
0 to E
0 to S

Figure S4

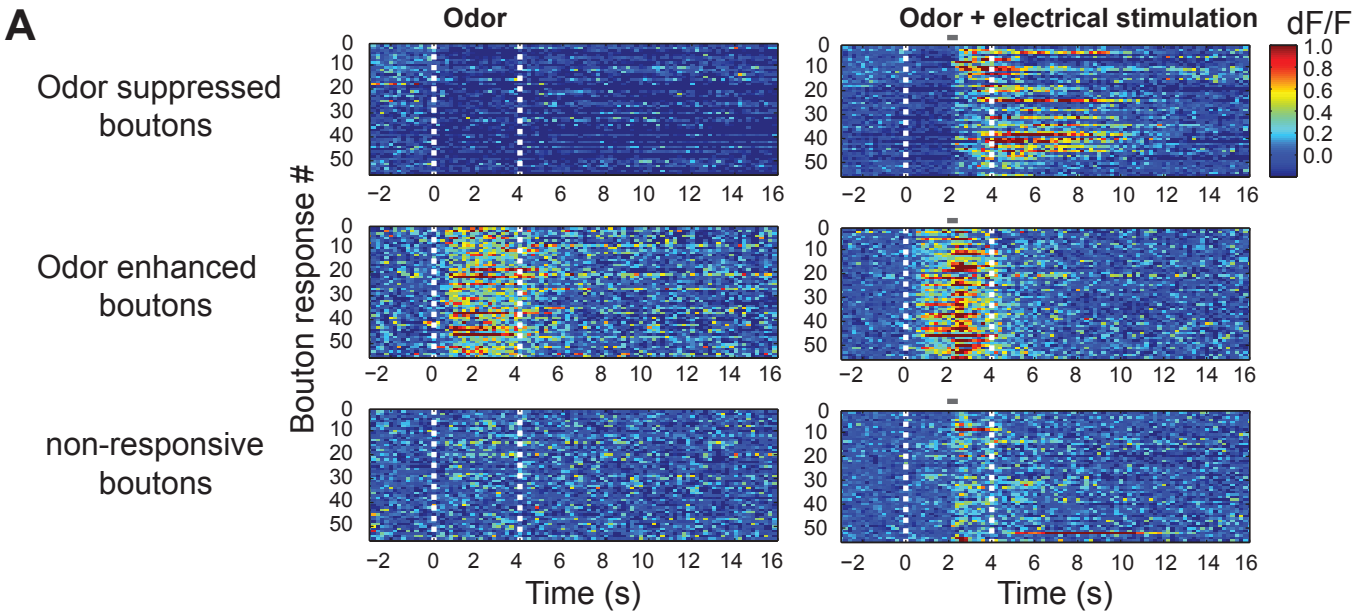
A
Odor
Odor + electrical stimulation
dF/F
Odor suppressed boutons
Odor enhanced boutons
non-responsive boutons
Bouton response #
Time (s)
Time (s)

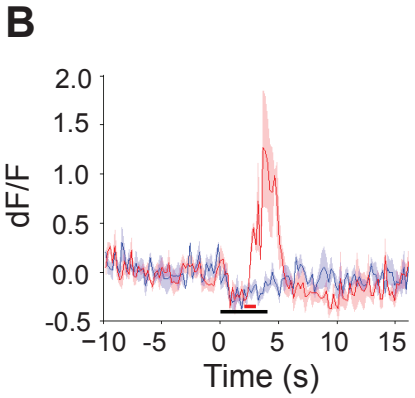
B
dF/F
Time (s)

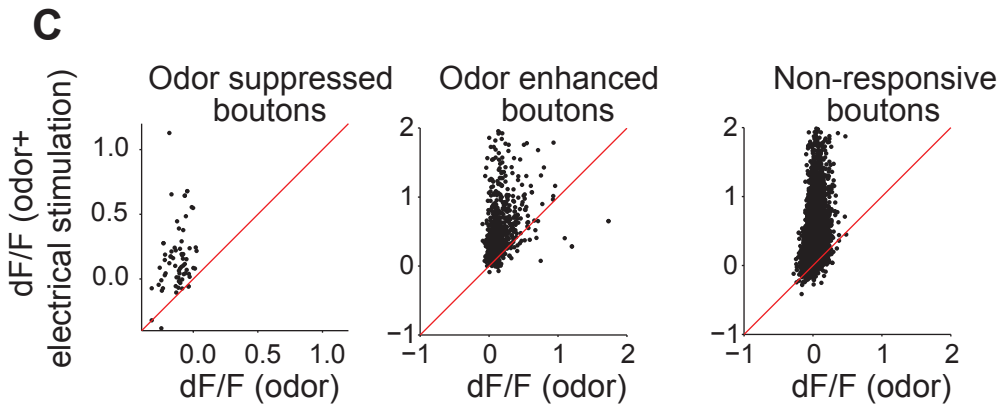
C
Odor suppressed boutons
Odor enhanced boutons
Non-responsive boutons
dF/F (odor+ electrical stimulation)
dF/F (odor)
dF/F (odor)
dF/F (odor)

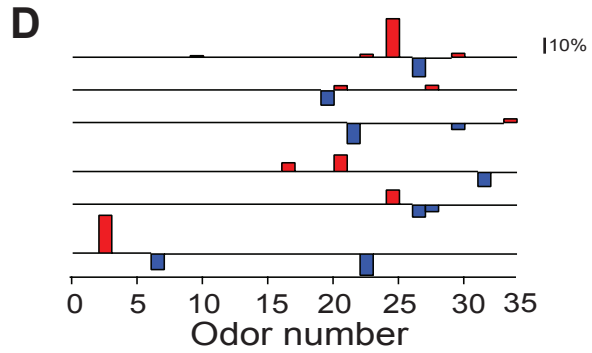
D
10%
Odor number

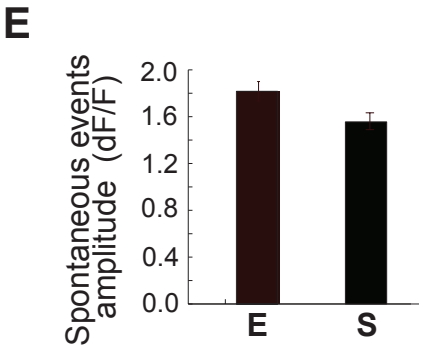
E
Spontaneous events amplitude (dF/F)
E
S

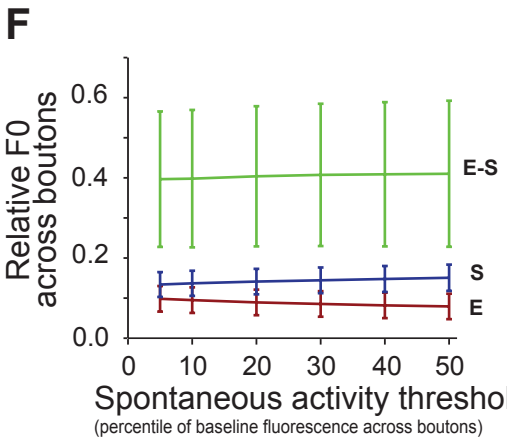
F
Relative F0 across boutons
E-S
S
E
Spontaneous activity threshold
(percentile of baseline fluorescence across boutons)

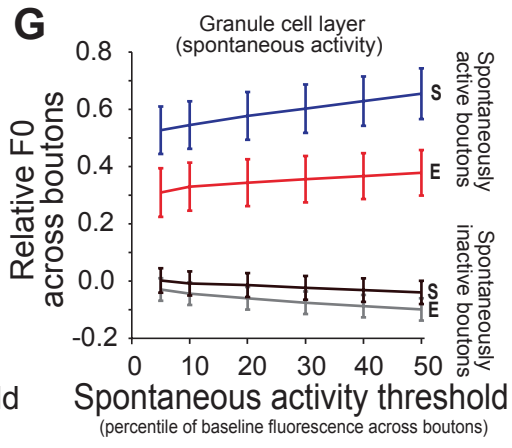
G
Granule cell layer
(spontaneous activity)
Relative F0 across boutons
Spontaneously active boutons
Spontaneously inactive boutons
S
E
S
E
Spontaneous activity threshold
(percentile of baseline fluorescence across boutons)

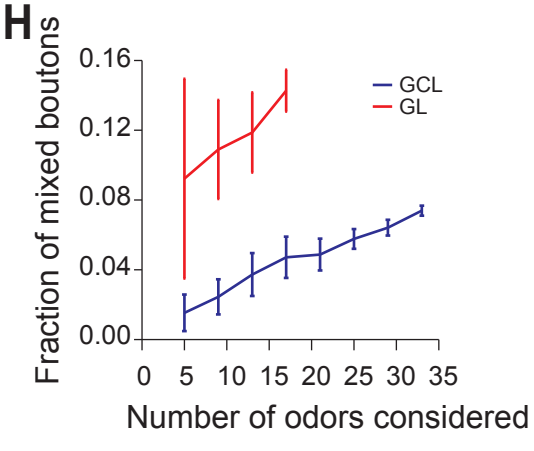
H
Fraction of mixed boutons
GCL
GL
Number of odors considered

Figure S5

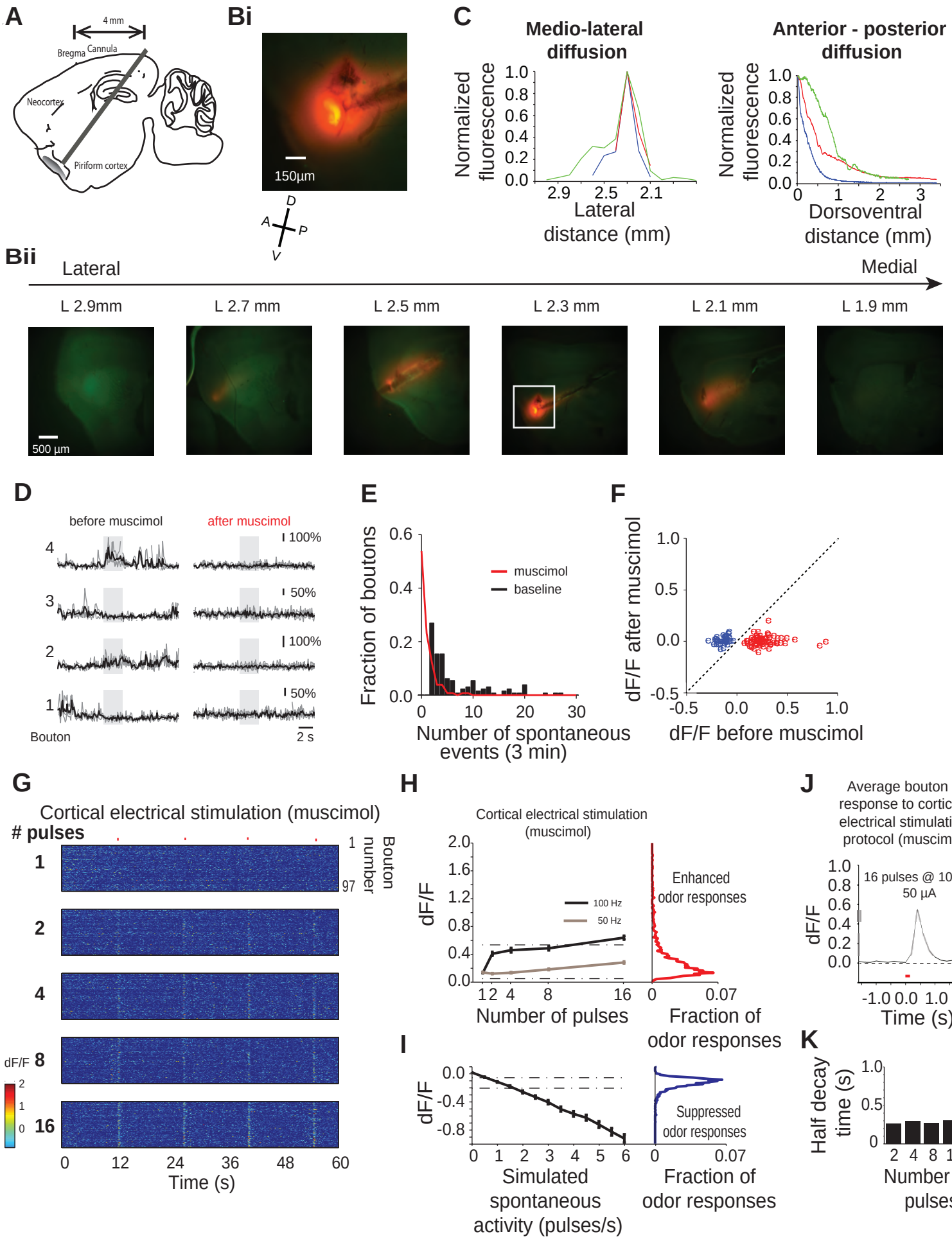
A
4 mm
Bregma
Cannula
Neocortex
Piriform cortex
Bi
150µm
D
A
P
V
C
Medio-lateral diffusion
Normalized fluorescence
1.0
0.8
0.6
0.4
0.2
0.0
2.9
2.5
2.1
Lateral distance (mm)
Anterior - posterior diffusion
Normalized fluorescence
0
1
2
3
Dorsoventral distance (mm)
Bii
Lateral
Medial
L 2.9mm
L 2.7 mm
L 2.5 mm
L 2.3 mm
L 2.1 mm
L 1.9 mm
500 µm
D
before muscimol
after muscimol
4
3
2
1
100%
50%
100%
50%
Bouton
2 s
E
Fraction of boutons
0.6
0.4
0.2
0.0
muscimol
baseline
0
10
20
30
Number of spontaneous events (3 min)
F
dF/F after muscimol
1.0
0.5
0.0
-0.5
-0.5
0.0
0.5
1.0
dF/F before muscimol
G
Cortical electrical stimulation (muscimol)
pulses
1
2
4
8
16
1
97
Bouton number
dF/F
2
1
0
0
12
24
36
48
60
Time (s)
H
Cortical electrical stimulation (muscimol)
dF/F
2.0
1.6
1.2
0.8
0.4
0.0
100 Hz
50 Hz
Enhanced odor responses
12 4
8
16
0
0.07
Number of pulses
Fraction of odor responses
J
Average bouton response to cortical electrical stimulation protocol (muscimol)
16 pulses @ 100 Hz
50 µA
dF/F
1.0
0.8
0.6
0.4
0.2
0.0
-1.0 0.0 1.0 2.0
Time (s)
I
dF/F
0.0
-0.4
-0.8
Suppressed odor responses
0 1 2 3 4 5 6
0
0.07
Simulated spontaneous activity (pulses/s)
Fraction of odor responses
K
Half decay time (s)
1.0
0.5
0
2 4 8 16
Number of pulses

Figure S6

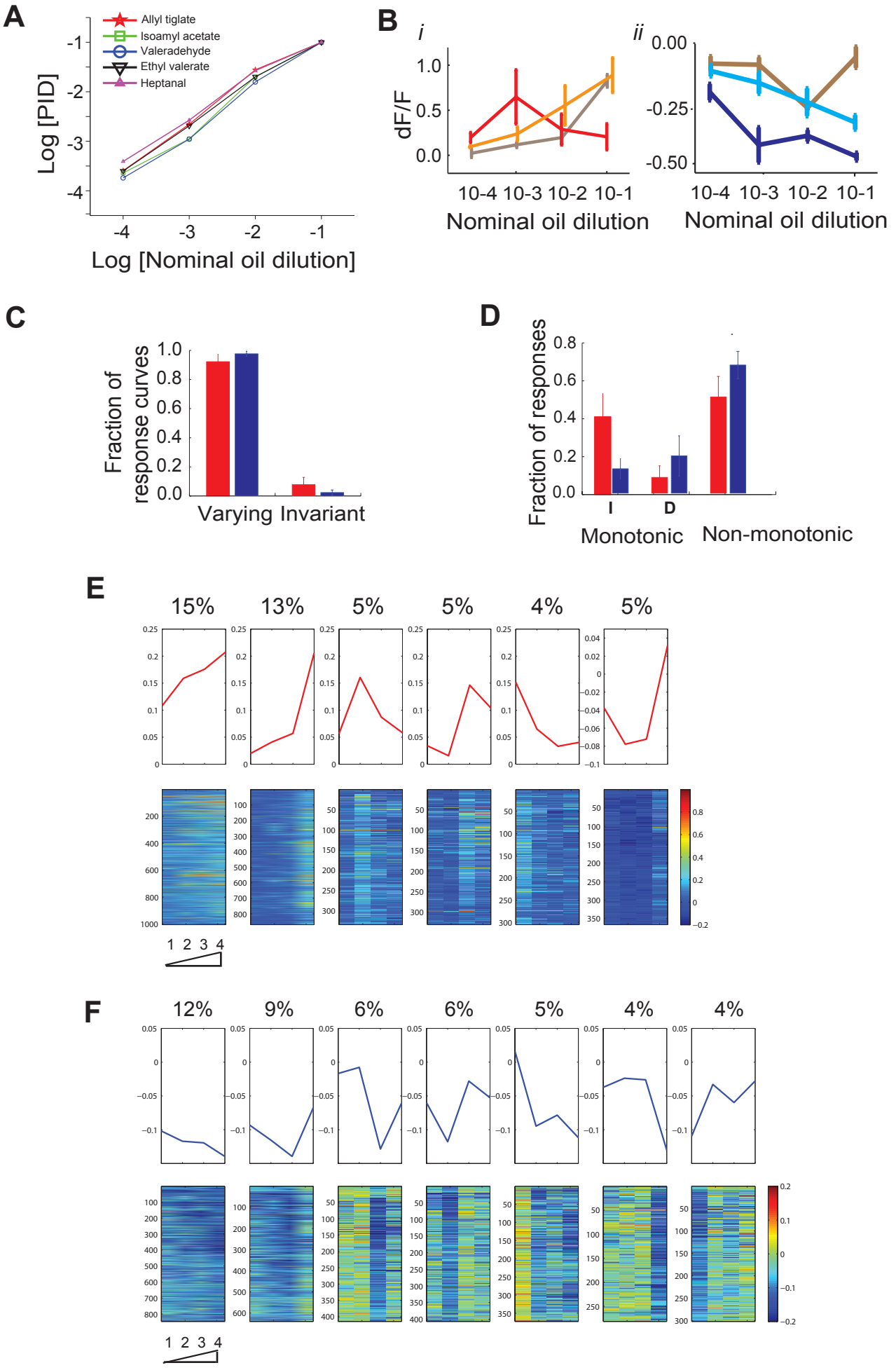
A
Allyl tiglate
Isoamyl acetate
Valeradehyde
Ethyl valerate
Heptanal
Log [PID]
Log [Nominal oil dilution]
B
i
ii
dF/F
Nominal oil dilution
Nominal oil dilution
C
Fraction of response curves
Varying
Invariant
D
Fraction of responses
I
D
Monotonic
Non-monotonic
E
15%
13%
5%
5%
4%
5%
1 2 3 4
F
12%
9%
6%
6%
5%
4%
4%
1 2 3 4

Figure S7

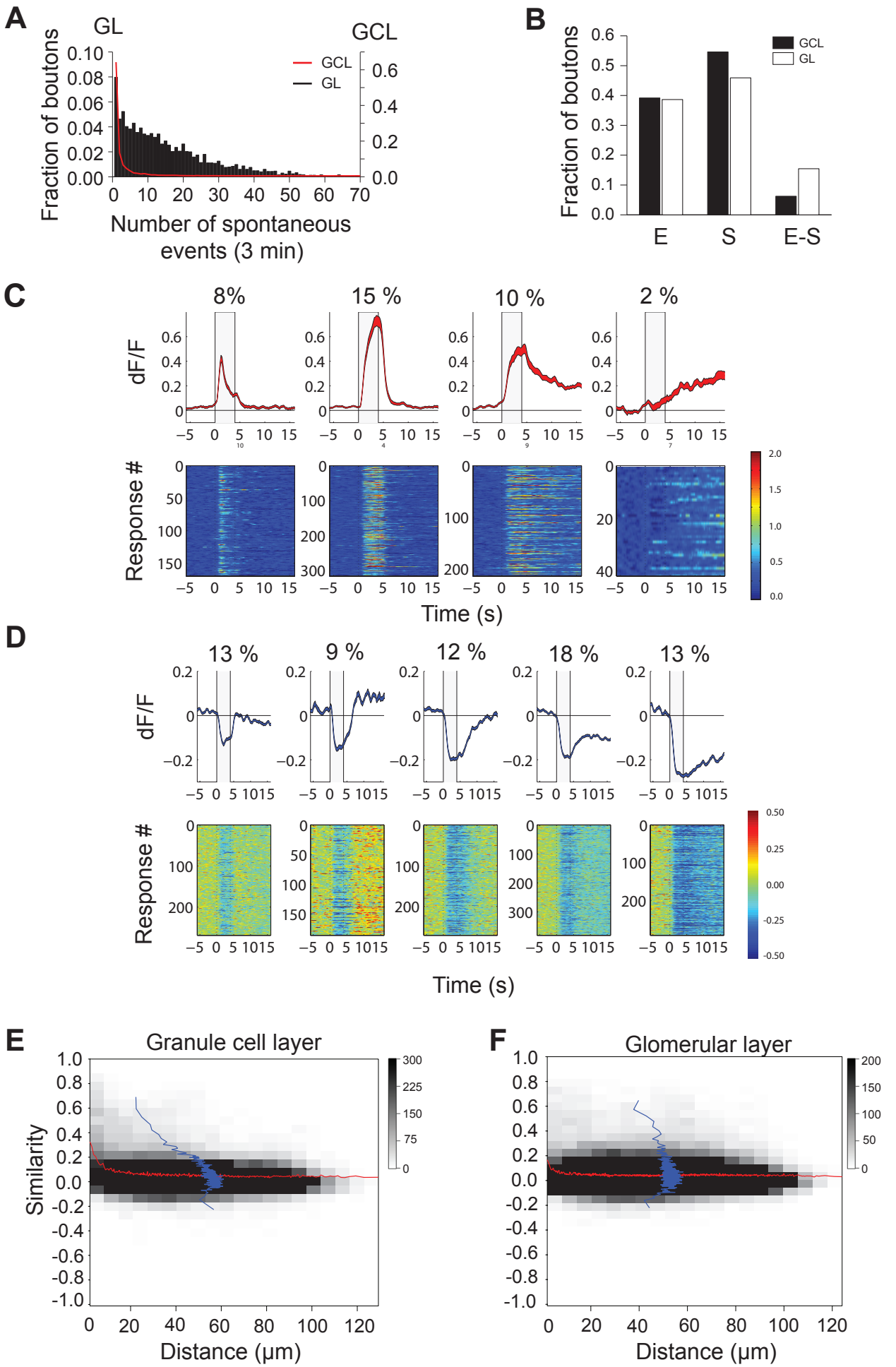
A
GL
GCL
Fraction of boutons
GCL
GL
Number of spontaneous events (3 min)
B
Fraction of boutons
GCL
GL
E
S
E-S
C
8%
15 %
10 %
2 %
dF/F
Response #
Time (s)
D
13 %
9 %
12 %
18 %
13 %
dF/F
Response #
Time (s)
E
Granule cell layer
Similarity
Distance (μm)
F
Glomerular layer
Distance (μm)

Figure S8

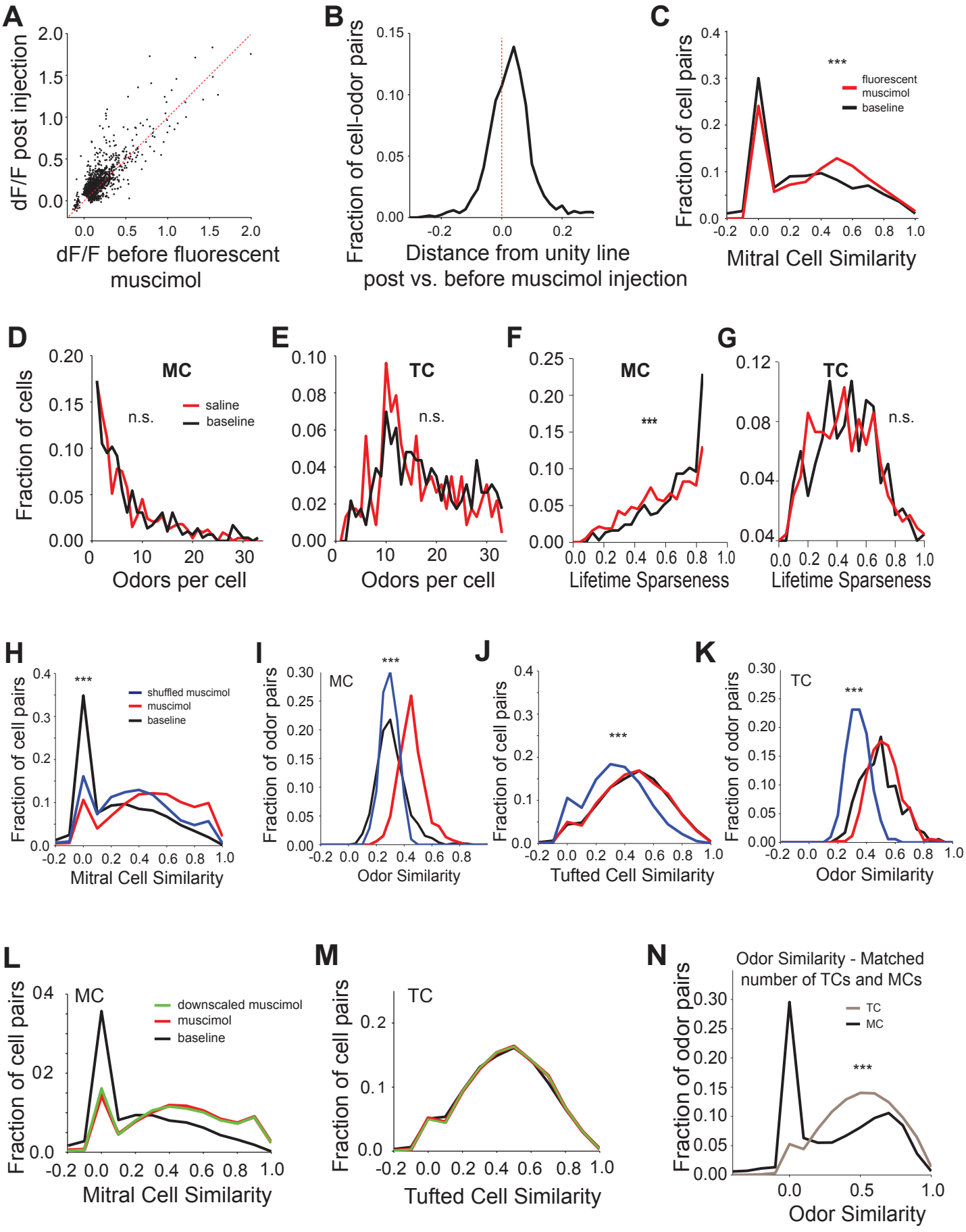
A
dF/F post injection
dF/F before fluorescent muscimol
B
Fraction of cell-odor pairs
Distance from unity line
post vs. before muscimol injection
C
Fraction of cell pairs
***
fluorescent muscimol
baseline
Mitral Cell Similarity
D
MC
n.s.
saline
baseline
Fraction of cells
Odors per cell
E
TC
n.s.
Odors per cell
F
MC
***
Lifetime Sparseness
G
TC
n.s.
Lifetime Sparseness
H
***
shuffled muscimol
muscimol
baseline
Fraction of cell pairs
Mitral Cell Similarity
I
MC
***
Fraction of odor pairs
Odor Similarity
J
***
Fraction of cell pairs
Tufted Cell Similarity
K
TC
***
Fraction of odor pairs
Odor Similarity
L
MC
downscaled muscimol
muscimol
baseline
Fraction of cell pairs
Mitral Cell Similarity
M
TC
Fraction of cell pairs
Tufted Cell Similarity
N
Odor Similarity - Matched number of TCs and MCs
TC
MC
***
Fraction of odor pairs
Odor Similarity

Supplemental Items Legends

Figure S1 relates to Figure 1 and Experimental Procedures.

Figure S2 relates to Experimental Procedures.

Figure S3 relates to Figure 1.

Figure S4 relates to Figure 1.

Figure S5 relates to Experimental Procedures and Figures 5-7.

Figure S6 relates to Figure 2.

Figure S7 relates to Figures 3 and 4.

Figure S8 relates to Figures 5-7.

Movie S1: "Corticalbulbar feedback boutons spontaneous activity" refers to Figure 1.

Movie S2: "Example corticalbulbar feedback boutons enhanced and suppressed responses to ethyl tiglate" refers to Figure 2.

Movie S3: "Example corticalbulbar feedback boutons enhanced and suppressed responses to acetal" refers to Figure 2.

Movie S4: "Example mitral cells responses to 4-heptanone before and after suppression of piriform cortex via muscimol" refers to Figure 5.

Movie S5: "Example tufted cells responses to methyl tiglate before and after suppression of piriform cortex via muscimol" refers to Figure 6.

Table 1 refers to Experimental Procedures.

Supplemental Note 1 refers to Experimental Procedures.

Supplemental Figure Legends

Figure S1. Viral labeling of corticobulbar feedback axons and algorithms for motion detection during imaging in awake head-fixed mice.

A. GCaMP5 expression in APC cell bodies: DAPI nuclear (blue) signals, cytosolic GCaMP5 (green) and composite of the two from confocal single optical slice (*Top*) and maximum projection (*Bottom*) reconstructions; fixed sagittal brain slice from a mouse injected into the anterior piriform cortex (APC) with AAV GCaMP5 expressing viruses;

B. Lack of GABAergic APC projections to the OB: composite DAPI nuclear (blue) signals and cytosolic GCaMP5 (green) images from fixed sagittal slices in APC and OB (GL, MCL and GCL) in a *GAD65*-Cre mouse injected with an *EF1-DIO-GCaMP5* AAV virus in the APC;

C. (*Left*) Example OB sagittal slice from a mouse infected with GCaMP5 in the anterior piriform cortex; (*Right*) zoom-in to glomerular layer (GL), external plexiform layer (EPL) and granule cell layer (GCL);

D. Density of fluorescently labeled (GCaMP5) boutons in the GL, EPL and GCL (boutons/μm^2); solid bars – fixed tissue; open bars – *in vivo*;

E. Example field of view in the granule cell layer and example single bouton (inset) for motion detection analysis; average reference (*Top*), as well as stable (*Bottom Left*) and x-y-z shifted frame (*Bottom Right*) are shown;

F. Uncentred correlation coefficient for each ROI between the average reference and individual frames across the duration of the trial; 0 marks the start of odor presentation; color scalebar shows correlation values;

G. Population stability for the field of view shown in E, during the same example trial, defined as the median of the distribution of correlation coefficients across all ROIs in the field of view; dotted line marks the threshold for determining x-y-z movement; note deflections below threshold classified as motion artifacts by the algorithm;

H. (*Left*) Example field of view ~300 µm deep from OB surface of GCaMP5 labeled cortical feedback axons and boutons in an awake head-fixed mouse; (*Right*) Spontaneous activity traces (dF/F_0) from the feedback boutons marked in the example FOV. Top five traces and respectively bottom three traces are from boutons assigned to two axonal branches by reconstruction of single axons;

Figure S2. Strategies for detection of spontaneous events and significant odor responses in corticobulbar feedback boutons.

A. Example normalized spontaneous fluorescence fluctuations (arbitrary units) from an example feedback bouton during a three minutes period preceding odor presentation; dotted red line indicates the threshold for detection of spontaneous events;

B. Histogram of fluorescence values (arbitrary units) in the time interval shown in **A**. (black bars) and log-normal distribution fit (red trace).Vertical red bar marks the 99th percentile of the fitted distribution and represents the detection threshold for spontaneous events; F_0 is the median of the fluorescence signal in the recorded interval;

C, D. Example spontaneous fluorescence fluctuations across 60 repeats of one enhanced (**C**) and one suppressed (**D**) feedback bouton during a 10 seconds period preceding odor presentation, as well as during three repeats of same stimulus presentation (4 s) and recovery period (12s).

E, **F**. Histogram of values (arbitrary units) in the pre-odor intervals shown in **C.** and **D**. Red bars correspond to the 99.9^{th} /0.1^{th} percentile of the recorded spontaneous fluorescence fluctuations distribution and represent the signal threshold. Blue bars mark the average single trial fluorescence during odor presentation;

G. Histogram of the number of odors that individual feedback boutons imaged in the GCL responded to (black bars) and binomial fit (red line).

H. Logarithmic plot showing the relationship between average number of odors per bouton data (black bars) shown in **G.** and the binomial fit (red line); note underestimation of the fraction of boutons responding to more than two odors by the binomial fit;

Figure S3. Awake versus anesthetized corticalbulbar feedback bouton responses

A. Responses of three example feedback boutons in an awake vs. lightly anesthetized mouse; Individual trials (gray) and average trace (black) are shown; shaded box marks odor presentation (4s);

B. Histogram of average number of spontaneous events (dF/F_0) detected in three minute intervals preceding odor stimulation in the awake (black) and anesthetized (red) conditions;

C. Scatter plot showing odor induced changes in bouton fluorescence (dF/F) in awake vs. anesthetized conditions; each dot indicates the response of a given bouton to a given odor (bouton-odor pair) in the awake versus anesthetized condition; only bouton-odor pairs that were detected as significant in at least one of the two conditions are shown; dotted line marks slope of

1; colors indicate bouton responses that were classified as suppressed (blue) and enhanced (red) in the awake condition;

D. Summary of changes in enhanced (E, *Left*) suppressed (S, *Center*) and unresponsive (0, *Right*) feedback bouton fraction of odor responses between awake and anesthetized conditions; E to S, enhanced to suppressed transitions, S to E, suppressed to enhanced response transitions, 0 to E, unresponsive to enhanced response transitions;

Figure S4A-C. Characterization of responses of odor enhanced, suppressed and non-responsive feedback boutons to APC electrical stimulation. Comparison of spontaneous fluorescence of enhanced vs. suppressed feedback boutons.

A. Average responses (3 repeats) of 58 example boutons to 'odors' (*Left*) and 'odor + brief cortical electrical stimulation' (8 pulses, 100μs at 100Hz) (*Right*) delivered interleaved; (*Top*) Odor suppressed boutons; (*Middle*) Odor enhanced boutons; (*Bottom*) Non-responsive boutons to odors in the panel; dotted white lines mark odor stimulation; red line marks electrical stimulation;

B. Example bouton response to an 'odor' (blue) and 'odor + cortical electrical stimulation' (red); note switch of response polarity from 'suppressed' to 'enhanced'; black line marks odor stimulation; red line marks electrical stimulation;

C. Scatter plots showing odor induced change in bouton fluorescence (dF/F) in the absence and presence of cortical electrical stimulation; each dot indicates the response of a given bouton to a given odor (bouton-odor pair) in the absence versus presence of cortical electrical stimulation; red line marks slope of 1;

D. Example odor response spectra of six feedback boutons showing both enhancement, as well as suppression of baseline activity in response to presentation of odors (Odor Set B, Table S1);

E. Average amplitude of spontaneous events excursions from baseline fluorescence (F_0) for odor enhanced (E) and respectively suppressed (S) boutons;

F. Relative baseline fluorescence (F_0), (see Methods) as a function of varying the detection threshold for spontaneous events; relative baseline fluorescence for enhanced (red), suppressed (blue) and mixed (green) boutons are shown; 640 suppressed, 564 enhanced, 41 mixed boutons; error bars represent SEM across boutons;

G. Relative baseline fluorescence (F_0) as a function of varying the detection threshold for boutons classified as spontaneously active (top two traces) and spontaneously inactive (bottom two traces); Relative baseline fluorescence (F_0) corresponding to spontaneously active and odor enhanced (red, 165 boutons), spontaneously active and odor suppressed (blue, 214 boutons), spontaneously inactive and odor enhanced (gray, 399 boutons) and spontaneously inactive, odor suppressed (black, 426 boutons) boutons are shown; error bars represent standard deviation of the mean across boutons, SD;

H. Average percentage of odors in the panel (Odor Set A and B, Table S1) a given mixed bouton responds to as a function of the number of odors presented; quantification for boutons in the GL (red) and GCL (blue) are shown; error bars represent standard deviation of the mean across boutons, SD.

Figure S5. Visualizing the spread of fluorescent muscimol injection, characterization of piriform cortex pharmacological suppression on feedback boutons activity, and

relationship between electrical stimulation and bouton fluorescence changes after piriform cortex inactivation.

A. Cartoon of sagittal brain slice illustrating the position of cannula used for muscimol infusion into APC; distance from the bregma is marked;

Bi. Spread of muscimol at the fluorescent muscimol injection site. **Bii.** Six representative slice examples, located 0.6 mm lateral to and 0.4 mm lateral from the fluorescent muscimol injection site (0), illustrating the position of the injection site within the APC and spread of red fluorescent muscimol; A-anterior, P-posterior, D-dorsal, V-ventral;

C. Distribution of fluorescence intensity decay with increasing distance from the injection site for the medial-lateral axis (*Left*) and anterior-posterior axis (*Right*) normalized to average fluorescence at the injection site;

D. Responses of four example boutons before and after muscimol injection in the APC; Individual trials (gray) and average trace (black) are shown; shaded box marks odor presentation (4s);

E. Histogram of average number of spontaneous events detected in three minute intervals preceding odor stimulation before (black) and after (red) muscimol injection;

F. Scatter plot showing odor induced change in bouton fluorescence (dF/F) before and after muscimol injection; each dot indicates the response of a given bouton to a given odor (bouton-odor pair) before versus after drug injection; only bouton-odor pairs that were detected as significant in at least one of the two conditions are shown; dotted line marks slope of 1; colors indicate bouton responses that were classified as suppressed (blue) and enhanced (red) before muscimol injection;

G. Responses (dF/F) of 100 example cortical feedback boutons to 4 repeats of different cortical electrical stimulation protocols (1-16 pulses, 100μs at 100Hz);

H. (*Left*) Average bouton response amplitude to five protocols of cortical electrical stimulation in the presence of muscimol at 50Hz (grey) and 100Hz (black); (*Right*) Distribution of bouton fluorescence changes (enhanced responses, dF/F) to odors in the panel (Odor Set A, Table S1);

I. (*Left*) Estimate of suppression in baseline average fluorescence, given a range of different simulated spontaneous activity (by convolving the average bouton response to electrical stimulation with a Poisson pulse train, see Methods); (*Right*) Distribution of bouton fluorescence changes (suppressed responses, dF/F) to odors in the panel (Odor Set A, Table S1);

J. Average bouton fluorescence change in response to cortical electrical stimulation (16 pulses, 100μs, 100 Hz) in the presence of muscimol;

K. Offset kinetics (half decay time) of average bouton responses to four protocols of cortical electrical stimulation in the presence of muscimol.

Figure S6. Characterization of corticobulbar feedback responses across odor concentrations.

A. Log-log plot showing the relationship between nominal dilutions in mineral oil to relative odor concentrations in air measured using a photo-ionization detector (PID) device; different color traces represent different odors: allyl tiglate, isoamyl acetate, valeraldehyde, ethyl valerate and heptanal;

B. Enhanced (*i*) and suppressed (*ii*) concentration–response (GCaMP5) curves for three example boutons each to two different odors (*i*, *ii*) in cortical feedback boutons; error bars indicate SEM across repeats;

C. Fraction of varying and invariant bouton odor responses within the sampled concentration range; enhanced (red) and suppressed (blue) bouton responses are shown;

D. Fraction of monotonical and non-monotonical changes in odor response amplitude within the concentration range for individual boutons; enhanced (red) and suppressed (blue) bouton responses are shown; *I*, monotonically increasing responses with increasing concentration; *D*, monotonically decreasing responses with increasing concentration;

E, F. Odor concentration response curves types obtained using k-means clustering and their relative distribution in the population of cortical feedback boutons targeting GCL; Average response shapes (*Top*) and all corresponding odor responses (GCaMP5) assigned to each cluster (*Bottom*) **E.** Enhanced response clusters; **F.** Suppressed response clusters; Color scale bars indicate average dF/F;

Figure S7. Characterization of corticobulbar feedback responses in the glomerular layer of the olfactory bulb.

A. Histogram of average number of spontaneous events detected above fluorescence baseline (F_0) in a three minute interval preceding odor stimulation; distributions in the GCL (black bars) and GL (red trace) are shown;

B. Fraction of boutons that responded significantly to odors in the panel (Odor Set A, Table S1) via only enhancement (E), only suppression (S) and both enhancement and suppression (E-S) across all responsive boutons sampled in the granule cell layer, GCL (solid bars) and glomerular layer, GL (open bars).

C, D. Odor response types obtained via k-means clustering and their relative distribution in the population of feedback boutons targeting the GL; Average response shapes (*Top*) and all

corresponding odor responses (GCaMP5) assigned to each cluster (*Bottom*) **A.** Enhanced response clusters; **B.** Suppressed response clusters; Color scale bars indicate average dF/F;

E, F. Two-dimensional histogram of pairwise correlations between spontaneous activity fluctuations of individual boutons in the granule cell layer (**E**) and glomerular layer (**F**) versus their physical separation. Red, average similarity (pairwise correlation) across different inter-bouton distances; Blue, average inter-bouton distance across all similarity values of bouton pairs; Gray scale, number of pairs per bin.

Figure S8. Odor responsiveness and population correlations of mitral and tufted cells before and after muscimol (non-fluorescent and fluorescent) injection in the anterior piriform cortex (APC).

A. Scatter plots showing odor induced change in mitral cell body fluorescence (dF/F) before and after *fluorescent muscimol*; each dot indicates the response of a given cell to a given odor (cell-odor pair) before versus after drug injection; only cell-odor pairs that were detected as significant in at least one of the two conditions are shown; dotted line marks slope of 1;

B. Summary histogram showing change in odor evoked mitral cells responses upon *fluorescent muscimol* (black) injection compared to pre-injection baseline; the change for each mitral cell odor response (each dot in **G**) is quantified in terms of the Euclidian distance from the diagonal unity line (dotted line indicating slope of 1);

C. Histogram of pairwise cell similarity of mitral cells before (black, baseline) and after (red) *fluorescent muscimol* injection ('baseline' MC Similarity=0.29 ± 0.004 vs. 'post-fluorescent muscimol' MC Similarity = 0.38 ± 0.004, N = 6,048 MT- odor pairs); Odor Set B, Table S1; *** indicate significance level ($p<0.001$, Wilcoxon signed rank test);

D. Histogram of the number of odors that individual mitral cells responded to before (black trace) and after (red trace) saline injection; (Avg. number of odor responses per cell = 7.32 ± 0.02 pre-saline vs. 6.99 ± 0.02 post-saline, N = 333 MCs, 4 hemibulbs, Wilcoxon sign rank test, p=0.12);

E. Histogram of the number of odors individual tufted cells responded to before (black trace) and after (red trace) saline injection; (Avg. number of odor responses per cell = 17.40 ± 0.30 pre-saline vs. 15.63 ± 0.15 post-saline, N = 229 TCs, 4 hemibulbs, Wilcoxon sign rank test, p=1);

F. Histogram of lifetime sparseness values for individual mitral cells before (black trace) and after (red trace) saline (Avg. lifetime sparseness = 0.78 ± 0.01 pre-saline vs. 0.69 ± 0.01 post-saline, N = 375 MCs, 4 hemibulbs, Wilcoxon sign rank test, p< 0.001, **I**) injection; *** indicate significance level (p<0.001, Wilcoxon signed rank test);

G. Histogram of lifetime sparseness values for individual tufted cells before (black trace) and after (red trace) saline (Avg. lifetime sparseness = 0.47 ± 0.01 pre-saline vs. 0.45 ± 0.01 post-saline, N = 233 TCs, 4 hemibulbs, Wilcoxon sign rank test, p< 0.001, **K**) injection; *** indicate significance level (p<0.001, Wilcoxon signed rank test); n.s. – not significant;

H. Histogram of pairwise cell similarity of mitral cells before (black, baseline), after (red) muscimol injection, as well as shuffled odor index control (blue) after muscimol injection; *** indicate significance level (Avg. MC Similarity=0.49 ± 0.002 vs. Avg. Shuffled MC Similarity = 0.36 ± 0.001, N=27,391 MT- odor pairs. Wilcoxon signed rank test, p<0.001);

I. Histogram of pairwise odor similarity of mitral cells before (black) and after (red) muscimol injection, as well as shuffled cell index control (blue) after muscimol injection; *** indicate significance level (Avg. MC Odor Similarity = 0.45 ± 0.01 vs. Shuffled Avg. MC Odor Similarity = 0.29 ± 0.002, p<0.001, Wilcoxon signed rank test, p<0.001);

J. Histogram of pairwise cell similarity of tufted cells before (black, baseline) and after (red) muscimol injection, as well as shuffled odor index control (blue) after muscimol injection (Avg. TC Similarity = 0.47 ± 0.002 vs. Avg. Shuffled TC Similarity = 0.34 ± 0.004, 11,522 TC-odor pairs. Wilcoxon signed rank test, $p<0.001$);

K. Histogram of pairwise odor similarity of tufted cells before (black), after (red) muscimol injection and shuffled cell index control (blue) after muscimol injection; (Avg. TC Odor Similarity = 0.53 ± 0.003 vs. Shuffled Avg. MC Odor Similarity = 0.34 ± 0.003, $p<0.001$, Wilcoxon signed rank test); *** indicate significance level.

L. Histogram of pairwise cell similarity of mitral cells before (black, baseline), after (red) muscimol injection, as well as 'downscaled-muscimol' control (green, see Methods) after muscimol injection; Avg. MC Similarity Muscimol=0.44 ± 0.002 vs. Avg. MC Similarity Downscaled Muscimol = 0.43 ± 0.002, N=22,654 MC- odor pairs; Wilcoxon rank sum test, $p>0.05$);

M. Histogram of pairwise cell similarity of tufted cells before (black, baseline) and after (red) muscimol injection, as well as 'downscaled-muscimol' control (green) after muscimol injection (Avg. TC Similarity Muscimol = 0.46 ± 0.002 vs. Avg. TC Similarity Downscaled Muscimol = 0.46 ± 0.002, 9,532 TC-odor pairs. Wilcoxon ranksum rank test, $p > 0.05$);

N. Histogram of pairwise odor similarity of mitral cells (black, MC) and tufted cells (gray, TC) before muscimol injection matched in numbers in terms of cells considered per field of view (40 randomly picked cells per field of view, 9 fields of view per iteration, 20 iterations); *** indicate significance level (Avg. MC Odor Similarity = 0.31 ± 0.001,N=94,402 odor pairs vs. Avg. TC Odor Similarity = 0.50 ± 0.001, N=73,561 odor pairs, $p<0.001$, Wilcoxon rank sum test);

Supplemental Movies

Movie S1

Time series movie acquired for 3 minutes at 5Hz showing the spontaneous activity of cortical feedback boutons expressing GCaMP5 in an optical plane ~300 μm below surface; Speed is 12x real time. Imaging window is 120 μm X 120 μm.

Movie S2

Time series movie showing a single trial response of corticobulbar feedback boutons in the GCL to ethyl tiglate. Within the field of view, odor presentation evoked enhanced (red arrow) and suppressed responses (green arrow). White arrow marks a bouton that did not respond to the odor stimulus. Speed is 2x real time. Imaging window is 110 μm X 75 μm.

Movie S3

Time series movie showing a single trial response of corticobulbar feedback boutons in the GCL to acetal. Within the field of view, odor presentation evoked enhanced (red arrow) and suppressed responses (green arrow). White arrow marks a bouton that did not respond to the odor stimulus. Speed is 2x real time. Imaging window is 110 μm X 75 μm.

Movie S4

Time series movie showing a single trial response (10Hz) of GCaMP3 expressing mitral cells (~220 μm from surface) to 4-heptanone. Odor-evoked responses of mitral cells before (Top) and after (Bottom) muscimol injection in the anterior piriform cortex (APC). Speed is 1x real time. Imaging window is 480 μm X 300 μm.

Movie S5

Time series movie showing a single trial response (10Hz) of GCaMP3 expressing tufted cells (~140 μm from surface) to methyl tiglate. Odor-evoked responses of mitral cells before (Left) and after (Right) muscimol injection in the anterior piriform cortex (APC). Speed is 1x real time. Imaging window is 300 μm X 480 μm.

Table S1

Odor index	Odor Set A	Odor Set B	Concentration
1	Acetal	2,4 decadienal	Allyl tiglate
2	1,4 Cineole	Propyl tiglate	Isoamyl acetate
3	Gamma Terpinene	valeraldehyde	Valeraldehyde
4	p-anis aldehyde	2,3-Pentanedione	Ethyl Valerate
5	Hexanal	Ethyl hexanoate	Heptanal
6	Methyl piruvate	Allyl butyrate	
7	Heptanal	Ethyl valerate	
8	Ethyl tiglate	2,3-Diethylpyrazine	
9	Valeraldehyde	hexanal	
10	2,3 pentanedione	Ethyl heptanoate	
11	Allyl tiglate	heptanal	
12	Ethyl propionate	Allyl tiglate	
13	1,4 dimethoxybenzene	ethyl tiglate	
14	Verbenone	Isoamyl acetate	
15	Ethyl butyrate	Methyl tiglate	
16	Citral	ethyl 3-mercapto propionate	
17	Ethyl valerate	4-heptanone	
18	(S)-limonene	gamma terpinene	
19	Ethyl caproate	Ethyl propionate	
20	Isoamyl acetate	acetal	
21		Ethyl butyrate	
22		1-pentanol	
23		acetophenone	
24		cyclohexyl acetate	
25		4-isopropyl benzaldehyde	
26		propyl acetate	
27		1-propanethiol	
28		cineole	
29		2-hexanone	
30		isobutyl propionate	
31		Hexanoic acid	
32		1,3 dimethoxybenzene	
33		valeric acid	

Supplemental Note 1

Cortical feedback boutons responded to odors either via either enhancement or suppression of baseline fluorescence, the mixed boutons (showing both enhanced, as well as suppressed responses) being a small minority. Could this dichotomy be explained simply by baseline saturation (due to high spontaneous activity) in the case of suppressed boutons which may prevent the detection of enhanced odor responses? Or, alternatively, by low fluorescence baseline in the case of enhanced boutons which would make the detection of small odor suppressed responses challenging? Several lines of evidence suggest that these issues are unlikely explanations for the observed response dichotomy across cortical feedback boutons.

a) in both enhanced and suppressed boutons, we observed robust spontaneous excursions in three minutes intervals recorded before odor stimulation (for both types, Avg. Amplitude of spontaneous events > 150 % dF/F_0) with respect to resting fluorescence (F_0) (Figure S4E); therefore, the baseline fluorescence signal is not already saturated at rest in the case of the suppressed boutons and affords in principle the detection of positive deflections;

b) Baseline fluorescence (F_0) was on average higher for suppressed vs. enhanced boutons, consistent with our observation of higher levels spontaneous activity in the suppressed boutons and the conservative threshold chosen for the detection of 'spontaneous events'; if a high pedestal of baseline fluorescence is an important limitation in the detection of 'enhanced' responses, then it is expected that on average the baseline fluorescence of mixed boutons (showing both types of responses) lies between that of purely suppressed and purely enhanced boutons. This was not the case: consistently, mixed boutons displayed on average higher baseline fluorescence (F_0) compared to both suppressed and enhanced boutons, irrespective of the detection threshold chosen for calling 'spontaneous events' (Figure S4F);

c) baseline fluorescence (F_0) was on average lower for boutons classified as spontaneously inactive vs. active, which may reflect the conservative nature of our detection threshold; importantly, baseline fluorescence of 'spontaneously active enhanced boutons' was higher than that of 'spontaneously inactive suppressed boutons', suggesting that the baseline fluorescence of 'spontaneously active enhanced boutons' was in principle high enough to afford the detection of suppressed odor responses had there been any (Figure S4G);

d) cortical feedback boutons in the glomerular layer showed robust spontaneous activity, more so than boutons in the granule cell layer (GCL); however, the feedback boutons in the glomerular layer were significantly sparser in suppressed odor responses compared to those in the GCL. The higher frequency of spontaneous events in the glomerular layer can be in principle related to differences in laser power and ease of optical access to the glomerular layer. Had high baseline fluorescence been a determining factor for detecting suppressed events, it is expected that the feedback boutons in the GL showed an increased frequency of suppressed odor responses, due to superior detectability. In fact, suppressed responses in the GL were sparser compared to those in the GCL (Figure 3D).

Experimental Procedures

Surgical Procedures: Adult mice (males and females >30 days old, 25-40 g) were anesthetized with ketamine/xylazine (KX, initial dose 70/7 mg/kg), further supplemented to keep the pedal withdrawal reflex suppressed. Lidocaine was applied topically at the site of surgical incision. Temperature was maintained at 37^{o} C using a heating pad (FST TR-200, Fine Science Tools, USA). Respiratory rate and lack of pain reflexes were monitored throughout the experiment. After the animal was deeply anesthetized, it was mounted in a stereotaxic frame with ear bars. Lidocaine and iodine were applied topically to skin (as analgesic and antiseptic, respectively). Aseptic technique was used, first clipping hair and prepping with betadine on the skin. Eyes were covered using paralube. A small incision (2-3 cm) was made into the skin above the surgical site.

Viral expression of GCaMP5 in the anterior piriform cortex (APC): To ensure spatially homogeneous expression, we performed three injections in each piriform cortex hemisphere, along the A-P and M-L axes (1.5 mm lateral, 2.8 mm anterior with respect to bregma, 3.0 mm deep from surface; L 2.0 mm, A 2.2 mm, D 3.5 mm; and respectively L2.5 mmm, A1.8 mm, D 4.0 mm). Post hoc, each imaged brain was perfused in PFA and GCaMP5 expression in the APC and OB assayed in sagittal slices via confocal imaging.

Chronic windows and head-fixed awake multiphoton imaging: Animals were anesthetized as described before and administered dexamethasone (4 mg/Kg) to prevent swelling, enrofloxacin against bacterial infection (5 mg/Kg), and carprofen (5 mg/Kg) to reduce inflammation. To expose the dorsal surface of the OB for chronic imaging, a small craniotomy was made over both OB hemibulbs, using a either a biopsy punch(Adam & Mizrahi, 2011) or thinning the skull with

a high-speed dental drill (Foredom, Bethel, CT), and removing it completely. A 3 mm glass cover slip (CS-3R, Warner Instruments) was placed atop and sealed in place using Vetbond (3M), further reinforced with cyanoacrylate (Krazy Glue) and dental acrylic (Lang Dental). A custom-built titanium head-bar was cemented on the skull near the lambda suture. To increase stability, the head-bar was designed to also contact the skull above the nasal passage, rostral to the OB. During the imaging sessions, the animal's head was held firmly in place by mounting the titanium headbar onto a custom-built holder. Carprofen (5 mg/Kg) was administered for two days following surgery. Animals were left to recover for at least 48 hours after surgery before imaging. GCaMP5 fluorescence was monitored by acquiring optical sections at different depths spanning from the glomerular (65-90 μm from surface) to the granule cell layers (200-350 μm from surface).

Multiphoton imaging: A Chameleon Ultra II Ti:Sapphire femtosecond pulsed laser (Coherent) was coupled to a custom built multiphoton microscope. The shortest optical path was used to bring the laser onto a galvanometric mirrors scanning system (6215HB, Cambridge Technologies). The scanning system projected the incident laser beam tuned at 930 nm through a scan lens (50 mm FL) and tube lens (300 mm FL) to backfill the aperture of the objective. An Olympus 20X, 1.0 NA objective was used for mitral and tufted cell imaging and an Olympus 25X, 1.05 NA for cortical feedback boutons imaging. A Hamamatsu modified H7422-40 photomultiplier tube was used as photo-detector and a Pockels cell (350-80 BK, 302RM driver, ConOptics) as beam power modulator. The current output of the PMT was transformed to voltage, amplified (SR570, Stanford Instruments) and digitized using a data acquisition board that also controlled the scanning (PCI 6115, National Instruments). Image acquisition and scanning (5-10 Hz) were controlled using custom-written software in Labview (National

Instruments). Using submicroscopic beads (0.5 μm) and a 1.05 NA, 25X Olympus objective, the point spread function (PSF) was calculated x-y (1.0 μm FWHM) and z (2.0 μm FWHM). Cortical feedback boutons were imaged across fields of view of either 120 x 120 μm (0.46 μm pixel size) or 60 x 60 μm (0.23 μm pixel size).

Recording procedure: Animals were head-fixed and habituated under the microscope to odors and the sound of the scanning galvos (45 min). Laser power was adjusted to minimize bleaching (<40 mW). For each field of view, 3 minutes of data were acquired before starting odor stimulation.

Data analysis

ROI selection and removal of z-plane motion artifacts

ROIs were manually drawn for individual boutons (0.9-3 μm diameter) in ImageJ using anatomical details from a reference median projection obtained from the 3 minute interval described above. For mitral and tufted cells imaging sessions, ROIs were manually selected based on anatomy. Care was taken to avoid selecting ROIs on cell bodies overlapping with neuropil (M/T lateral dendrites).

To detect fast z-plane movements that might occur across single frames, an average image was calculated using all frames for the given trial. Using this average image, each ROI was described as a vector of length equal to the total number of pixels within the ROI (r_{mean}). We further calculated corresponding vectors from the same ROI across each individual frame (r_{frame}). r_{mean} and r_{frame} were compared by calculating the cosine of the angle between the two vectors:

$$cos_{frame} = \frac{r_{mean} \cdot r_{frame}}{\sqrt{(r_{mean} \cdot r_{mean})(r_{frame} \cdot r_{frame})}}$$

This metric corrects for changes in brightness and only takes into account changes in shape. cos_{frame} has a value of 1, if the ROI in a particular frame is identical in shape to that in the average image, even if dimmer in intensity. If the ROI has a different shape, cos_{frame} approaches zero. Note that, because the ROIs were chosen slightly larger than individual boutons, they included both bright pixels that are part of a bouton, as well as dark pixels from surround. This allowed cos_{frame} to be very sensitive to lateral displacements or z-movements which inevitably change the distribution of bright and dark pixels within the drawn ROI. For each ROI, a time series of cos_{frame} was created that estimated the similarity in time of the bouton to the template average vector. Z-movement for a particular frame would produce a synchronized drop in cos_{frame} across a large number of boutons. We therefore estimated the *population stability* for a given frame as the median of the cos_{frame} calculated over all boutons in a field of view. The *population stability* was converted to a z-score by subtracting the mean population displacement from the air period preceding the odor presentation and dividing by the standard deviation of *population stability* during air. The air period was used to calculate the z-score since we observed only minimal z-movement during this interval. A drop of more than 2 z-scores was classified as a motion artifact and the entire corresponding frame discarded from any further analysis.

Detection of spontaneous events

During the air period, spontaneous increases in fluorescence occurred that deviated from the average fluorescence for a given bouton (ROI). To detect spontaneous events for a given ROI, a distribution of resting fluorescence was constructed, considering only the lower half of the

fluorescence values pooled across 3 minute intervals and fitting it with a log-normal distribution. We assumed that fluorescence values smaller than the median did not overlap with the spontaneous events to be detected, and we used the fitted log-normal distribution as proxy for the distribution of resting fluorescence (99th percentile as threshold for spontaneous events). A spontaneous event was defined as fluorescence transiently crossing the threshold and falling back again to resting values. A bouton was classified as spontaneously active, if at least two spontaneous events were observed during the 3 minute interval. Note that these events likely represent several action potentials and not individual spikes (Tian et al., 2009).

Estimation of relative baseline fluorescence – Figure S$F,G

Generally, the baseline fluorescence was estimated as the median of the distribution of fluorescence signals (50 percentile) for a given bouton. We verified that the analysis shown in Figure S4F and Figure S4G was unaffected even when the threshold was set to lower percentiles. Observed baseline fluorescence for a given field of view depends not only on the intrinsic resting activity, but also on other factors like laser power, tissue scattering etc. To allow comparisons of the estimated baseline fluorescence of boutons acquired across different fields of view, we defined the relative fluorescence of a given ROI in a given field of view as the z-score calculated over the population of all fluorescent boutons in the field of view.

Odor response analysis – detection of significant enhanced and suppressed responses

The distribution of fluorescence for a given ROI is in principle asymmetric, limited by saturation for increases, and 0 firing rate for decreases in fluorescence. Parametric tests of

significance that set symmetric thresholds as a number of standard deviations above and below the mean fluctuation would result in underestimating the significance of suppressed events. Given access to long periods of air recorded preceding odor presentations (20 odors * 4 repeats per odor *10 s per repeat = 800 s per imaging session), we calculated statistics that allowed determining with high confidence whether an increase or decrease in dF/F during odor presentation deviated from spontaneous fluctuations during baseline. We estimated a reference baseline fluorescence distribution by sliding a temporal window of same duration as odor presentation (4s) over the acquired air period and averaging the dF/F. This procedure was repeated 5,000 times to obtain a bootstrap estimate of the spontaneous fluorescence distribution. The response from a single odor repeat was considered 'significant enhancement', if it exceeded 99.9th percentile of the distribution, and respectively 'significant suppression', if it corresponded to less than 0.1th percentile. Note that this procedure is non-parametric, therefore solving the asymmetry problem. An odor was called to trigger significant enhancement (or suppression) for an individual ROI if it elicited responses across at least two repeats.

Functional clustering analysis

In addition to fluorescence changes whose significance was assessed over the 4 s odor period, we also assessed significance during the first 2 s, last 2 s, as well as 4 s following the end of odor presentation. These extra traces were included to capture potential rich temporal dynamics such as early adapting, delayed and OFF responses. The selected waveforms were smoothed using a 0.8 s moving average window and normalized by the absolute value of the largest magnitude response. We used the k-means clustering function in MATLAB (Euclidean distance). Cluster quality was assessed by calculating the average distance between waveforms assigned to a cluster (*d*). To determine the total number of clusters, we calculated the average *d*,

while varying the number of clusters from 2 to 30. The average decrease in *d* was further plotted as a function of increasing number of clusters. The total cluster number (10 for GCL and 9 for GL waveforms) was chosen using a cutoff where the average decrease in *d* plateaued.

Concentration analysis – invariant versus variant responses, monotonicity, clustering

For each ROI, the significance for each odor response at each concentration was assessed independently. An ROI was classified as concentration invariant only if it cleared significance at all four concentrations used and the magnitude of responses did not differ across concentrations. The response at each concentration was described as a vector of mean dF/F during odor period across trials. To construct a concentration response curve, the average dF/F across trials for each concentration was used. Variability across concentrations (q) was quantified as the standard deviation of the trial-averaged dF/F values. A family of concentration response curves was constructed by shuffling the concentration labels for the mean dF/F of individual trials and randomly assigning them to any of the four concentrations used. For each shuffle round, a q' value was obtained by calculating the standard deviation of the resulting concentration response curve. Repeating this procedure 100 times produced a null distribution of q' values. Concentration invariant ROIs were required to have a value of q between the 5th and 95th percentile of the q' distribution.

To establish whether an ROI showed monotonically increasing or decreasing responses to a given odor across concentrations, its concentration response curve (described above) was fitted with a line and its slope evaluated for monotonicity. All odor-ROI pairs that showed at least one significant response (across trials) to at least one of the concentrations were considered. To assess if such a slope could have arisen by chance, a null distribution of slopes (100) was created

by shuffling the concentration labels and calculating shuffled concentration response curves. A response was considered monotonically increasing if its slope was larger than the 95th percentile of the shuffled distribution, and monotonically decreasing if it smaller than the 5th percentile. Clusters of response concentration curves (13) were also calculated using k-means clustering.

Odor pair similarity using enhanced responses only vs. suppressed responses in GL and GCL

Cortical feedback boutons responses separated into boutons that responded only by enhancing or only by suppressing baseline fluorescence. We constructed two vector populations per odor: one using ROIs with purely enhanced responses and one using the purely suppressed ROIs to calculate the Pearson linear correlation coefficient. We also calculated the mutual information (I(e;s)) between the odor similarities obtained using the enhanced population responses versus suppressed responses. The mutual information is given by:

I(e;s)=H(e)+H(s)-H(e,s).

where:

H(e) - entropy of odor similarity distribution using the enhanced responses;

H(i) - entropy of odor similarity distribution using the suppressed responses;

H(e,s) - joint entropy of odor similarity of both enhanced and suppressed responses;

Entropies were given by:

$H(s) = \sum -p(odor\ similarity)\ log_2(p(odor\ similarity))$

All the distributions were estimated using a normalized histogram and using a bin size of 0.1.

To estimate whether the calculated mutual information was different from chance, we shuffled the odor identities and re-calculated the mutual information (10,000 times).

Shuffled correlation

To calculate shuffled cell similarity, the odor identities of the ORS of each of the two cells were randomly exchanged before calculating the cell similarity. For odor similarity, the cell identities of the population response vector (CRS) of each of the two odors were shuffled before calculating the similarity.

Odor similarity-matching number of mitral cells and tufted cell

To match the number of mitral cells and tufted cells used to construct population vectors, we randomly selected 9 fields of view in the mitral cell layer and 9 fields of view in the EPL containing tufted cells. To match the number of cells in each FOV, we pseudorandomly selected 40 mitral cells and 40 tufted cells. We chose 40 cells because it represented a lower bound of the average number of tufted cells imaged in a given FOV. We used a total set of 528 (odor pairs) X 9 (randomly selected FOVs) X 20 (repeats) and plotted the distribution of odor similarity by performing 20 iterations of randomly selecting 40 mitral and 40 tufted cells across 9 fields of view.

Pharmacology

Animals were implanted with cannulas in the APC using 26 Gauge cannula (Plastics One) at a 50 degree angle from the vertical (Figure S5A) at the same time as the optical window was implanted. Cannulae were implanted bilaterally, but muscimol/saline was injected in only one hemisphere per imaging session. After imaging a given field of view (baseline), muscimol (muscimol hydrobromide, MW=195.01, Sigma) dissolved in cortex buffer (0.5 mg/ml, injecting 1 μl over 5 min) was used to suppress activity in the piriform cortex. No apparent changes in the animals' sniffing, whisking or motor behaviors were observed upon muscimol injection. In a subset of experiments (N=3 mice), we used fluorescent muscimol bodipy (MW=607.46, Life

Science Technologies, 1mg/ml in cortex buffer and 5% DMSO, injected 2µl over 10 min). To account for differences in molecular weight between fluorescent and non-fluorescent muscimol, we injected higher volume of more concentrated drug solution in the fluorescent muscimol experiments. To quantify the spread of the drug, two hours post injection, animals were killed, perfused in PFA, and 100-200 µm sagittal slices were cut and imaged under an epifluorescence microscope. Fluorescent muscimol intensity was assayed at the injection site by calculating the mean fluorescence within a 200 x 200 µm ROI, centered at the site of the cannula tip and used as 'reference'. Across all imaged slices, same size ROIs were selected, centered at the site of highest fluorescence within each slice, and the calculated average fluorescence value normalized by the 'reference'. For control experiments (saline controls), only cortex buffer was used.

For experiments comparing feedback odor responses between awake and anesthetized conditions, a field of view was initially imaged while the animal was awake. The animal was then injected intraperitonealy with ketamine/xylazine (KX, 35/3.5 mg/kg) and lightly anesthetized, preserving strong pedal withdrawal reflex. We waited for 10 minutes after injection before continuing imaging in the same field of view. Care was taken to identify same feedback boutons in the FOV before and after anesthesia. Body temperature was maintained using a heating pad (FST TR200).

Anterior Piriform Cortex (APC) Electrical Stimulation

Animals were implanted with a guide cannula in the anterior piriform cortex (C315GS-4/SP, 26 G, 9 mm below pedestal, Plastics One, Figure S5A), through which an electrode (A-M Systems stainless steel wire, cat #790900, core diameter = 76.2 µm, coated diameter 139.7 µm) placed within an infusion Internal cannula (C315IS-4/SP, Plastics One) was inserted. A skull screw in the right parietal bone served as ground. The electrode tip was gold plated to an

impedance of <50 kΩ. Current pulses were delivered using an Isolated Pulse Stimulator 2100 (A-M Systems). For experiments described in Figure S4A-C (no muscimol), biphasic cathode-leading current pulses (100μs, <30 μA) were used. We did not observe a startle response in the animal at this level of current. For 'odor' and 'odor + electrical stimulation' experiments, we used a set of 20 odors (Odor Set A, Table S1) and followed same delivery protocols as described above; 'odor' and 'odor+electrical stimulation' trials were presented in a randomly interleaved manner. The current pulses (1, 2, 4, 8 or 16) were delivered either at 50Hz or 100Hz during the air period, or 2s from odor onset. Responsiveness for each ROI-odor pair was assessed based on odor presentation in the absence of electrical stimulation.

For experiments described in Figure S5G-K, activity in the APC was suppressed by injecting muscimol dissolved in cortex buffer (0.5 mg/ml, injecting 1 μl over 5 min) through an internal cannula. After muscimol injection, the internal cannula was replaced with the stimulating electrode. Given a steep reduction in number of boutons that responded to the electrical stimulation protocol post muscimol injection, current amplitude was increased to 50 μA to trigger detectable fluorescence changes. We used for further stimulation protocols only boutons that showed a significant response to a strong stimulus (100μs pulse train at 100Hz for 1s) duration. For the different protocols used (1, 2, 4, 8, 16 pulses at 50Hz or 100Hz), each stimulation train was presented 12 times, at 15 seconds ITI. To determine significance of responses to different stimulation trains, a 250 ms interval preceding the electrical was compared to a 250 ms interval after the pulse ($p<0.001$, paired t-test, 12 pulses, separated by 15 seconds).

Histology

Animals were perfused intracardially, the brains were preserved in PFA and sliced in the sagittal plane with 50-200 μm sections. Slices were mounted using VECTASHIELD Mounting Medium containing DAPI and imaged using a confocal microscope.

References

Adam, Y., & Mizrahi, A. (2011). Long-term imaging reveals dynamic changes in the neuronal composition of the glomerular layer. *The Journal of neuroscience*, *31*(22), 7967–73. doi:10.1523/JNEUROSCI.0782-11.2011

Tian, L., Hires, S. A., Mao, T., Huber, D., Chiappe, M. E., Chalasani, S. H., Petreanu, L., et al. (2009). Imaging neural activity in worms, flies and mice with improved GCaMP calcium indicators. *Nat Meth*, *6*(12), 875–881. doi:10.1038/nmeth.1398